Laser frequency stabilization using Mach-Zehnder interferometer

Department of Physics, The University of Tokyo 21527H

Satoshi Sakaguchi

Cooperative experimenter
Hiroshi Yahata

2003/9/18

Contents

List of Figures

List of Tables

Abstract

We have stabilized about 2 orders of laser frequency at the maximum in the 1 to 300Hz zone. Techniques of phase detection using Mach-Zehnder interferometer and phase fixation by 2-loop feedback were used for stabilization.

Chapter 1

Introduction

Although existence of a gravitational wave was predicted according to Einstein's general theory of relativity, it has not yet succeeded in direct detection. In this section, the theory of gravitational wave and the motivation to laser frequency stabilization are discussed.

1.1 Einstein equation

According to the general relativistic theory, senso between two points x^μ and $x^\mu + dx^\mu$ canbe expressed as follows using metric tensor $g_{\mu\nu}$.

$$ds^2 = g_{\mu\nu} dx^\mu dx^\nu. \tag{1.1}$$

In flat space-time without the gravitational field (Minkowski space-time), $g_{\mu\nu}$ is

$$g_{\mu\nu} = \eta_{\mu\nu}. \tag{1.2}$$

where

$$\eta_{\mu\nu} = \begin{pmatrix} -1 & 0 & 0 & 0 \\ 0 & 1 & 0 & 0 \\ 0 & 0 & 1 & 0 \\ 0 & 0 & 0 & 1 \end{pmatrix}. \tag{1.3}$$

Christoffel symbol $\Gamma^\mu_{\nu\lambda}$, Riemann tensor $R^\mu_{\nu\alpha\beta}$, Ricci scalar R are defined as follows.

$$\Gamma^\mu_{\nu\lambda} = \frac{1}{2} g^{\nu\alpha} (g_{\alpha\nu,\lambda} + g_{\alpha\lambda,\nu} - g_{\nu\lambda,\alpha}) \tag{1.4}$$

.

$$R^\mu_{\nu\alpha\beta} = \Gamma^\mu_{\nu\beta,\alpha} - \Gamma^\mu_{\nu\alpha,\beta} + \Gamma^\mu_{\gamma\alpha}\Gamma^\gamma_{\nu\beta} - \Gamma^\mu_{\gamma\beta}\Gamma^\gamma_{\nu\alpha}. \tag{1.5}$$

$$R_{\mu\nu} = R^{\alpha}_{\mu\alpha\nu}. \tag{1.6}$$

$$R = R^{\alpha}_{\alpha}. \tag{1.7}$$

In the time-space with the gravitational fields, metric tensor $g_{\mu\nu}$ follows Einstein equation Eq. (1.8). $T_{\mu\nu}$ is an energy momentum tensor.

$$G_{\mu\nu} = \frac{8\pi G}{c^4} T_{\mu\nu}. \tag{1.8}$$

where

$$G_{\mu\nu} = R_{\mu\nu} - \frac{1}{2} g_{\mu\nu} R - \Lambda g_{\mu\nu}. \tag{1.9}$$

1.2 Gravitational wave

Here, we consider the perturbation of the flat Minkowski metric $\eta_{\mu\nu}$

$$g_{\mu\nu} = \eta_{\mu\nu} + h_{\mu\nu}. \tag{1.10}$$

where $h_{\mu\nu}$ is a small perturbation of $\eta_{\mu\nu}$. We then define$\overline{h}_{\mu\nu}$,the trace reverse tensor of $h_{\mu\nu}$ as

$$\overline{h}_{\mu\nu} = h_{\mu\nu} - \frac{1}{2} \eta_{\mu\nu} h. \tag{1.11}$$

$$h = h^{\alpha}_{\alpha}. \tag{1.12}$$

Therefore, to first order in $|\overline{h}_{\mu\nu}|$, we have

$$G_{\mu\nu} = -\frac{1}{2} (\overline{h}^{,\alpha}_{\mu\nu,\alpha} + \eta_{\mu\nu} \overline{h}^{,\alpha\beta}_{\alpha\beta} - \overline{h}^{,\alpha}_{\mu\alpha,\nu} - \overline{h}^{,\alpha}_{\nu\alpha,\mu}). \tag{1.13}$$

In Lorentz gauge

$$\overline{h}^{\mu\nu}_{,\nu} = 0. \tag{1.14}$$

Eq. (1.13) is simplified as

$$G_{\mu\nu} = -\frac{1}{2} \Box \overline{h}_{\mu\nu}. \tag{1.15}$$

where

$$\Box = -\frac{\partial^2}{c^2 \partial t^2} + \triangle. \tag{1.16}$$

The Einstein eq. becomes

$$\Box \overline{h}_{\mu\nu} = -\frac{16\pi G}{c^4} T_{\mu\nu}. \tag{1.17}$$

Since $T_{\mu\nu} = 0$ in vacuum,

$$\Box \overline{h}_{\mu\nu} = 0. \tag{1.18}$$

As in electromagnetism, a solution to Eq. (1.17) is the retarded potential:

$$\overline{h}_{\mu\nu}(t, x) = \frac{4G}{c^4} \int \frac{T_{\mu\nu}(t - \frac{r'}{c}, x')}{r'} d^3x'. \tag{1.19}$$

A solution to Eq. (1.18) is the plane wave:

$$\overline{h}_{\mu\nu}(t, x) = A_{\mu\nu} e^{ik_\alpha x^\alpha}. \tag{1.20}$$

1.3 Gravitational wave detection

A gravitational wave is distortion of the space-time spread at the velocity of light. However, since this distortion is very feeble, direct detection is not yet made. Today, detection of a gravity wave is mainly tried using laser interferometers. The principle is simply as follows.

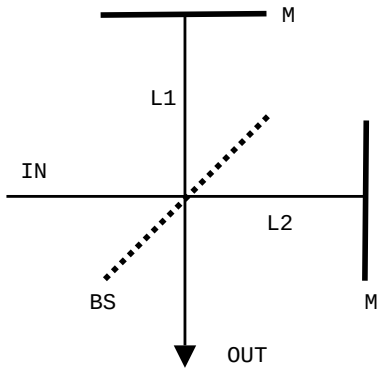

Figure 1.1: Michelson interferometer

The optical system of detectors is based on Michelson interferometer (Fig. 1.1). An optical path difference of two light pathes which intersected perpendicularly is observed as intensity change of interference light. Unlike the electric charge which is the source of an electromagnetic wave, the mass which is the source of a gravitational wave cannot take a negative value. For this reason, dipole radiation like an

electromagnetic wave does not exist for gravitational wave, and quadropole radiation is to be observed. Quadropole radiation of the distortion of space-time causes one optical path of the interferometer to get shorter, and the other to get longer. Therefore, we can detect optical path differences caused by gravitational waves.

1.4 Significance of laser frequency stability

To detect a very feeble signal of a gravitational wave, stability of laser frequency is quite important.

The electric field of incidence laser light is set to

$$E_{in} = E_0 e^{i\omega t}. \tag{1.21}$$

Incidence laser light is divided into two light in a beam splitter, change their phase to ϕ_1,ϕ_2 before interference. Thus, the output light is expressed as

$$E_{out} = \frac{1}{2}E_0 e^{i(\omega t-\phi_1)} - \frac{1}{2}E_0 e^{i(\omega t-\phi_2)}. \tag{1.22}$$

$$\begin{aligned} P_{out} &= \overline{|E_{out}|^2} && (1.23)\\ &= \frac{1}{2}|E_0|^2(1-\cos(\phi_1-\phi_2)) && (1.24)\\ &= \frac{1}{2}P_{in}(1-\cos\Delta\phi). && (1.25) \end{aligned}$$

where $\Delta\phi = \phi_1 - \phi_2$.

By measureing P_{out}, we can know the value of ϕ. Here, ϕ can be written as

$$\Delta\phi = \frac{2\pi\Delta L}{\lambda} = \frac{\omega\Delta L}{c}. \tag{1.26}$$

where ΔL is an optical path difference that changes with gravitational wave. Therefore, it is very important to keep the value of ω as stable as possible for gravitational wave detection.

Chapter 2

Principle

We have stabilized laser frequency using Mach-Zehnder interferometer. In this section, principle of frequency stabilization is discussed. First, we deal with the principle of feedback control. Then, the principle of stabilization is disscused in three subsections on optical system, Data taking system, and on Feedback system.

2.1 Feedback control

2.1.1 Transfer function

Laplace transform and transfer function

The function for treating transfer of a signal is defined. The input signal to a certain circuit element is set with x(t), and an out put signal is set with y(t). The Laplace transform to function of time f(t) is defined by the following definite integral.

$$F(s) = L[f(t)] = \int_0^\infty f(t)e^{-st}dt. \tag{2.1}$$

Here, it is referred to as f(t)=0 by t<0. s is complex.

Laplace transform of x(t) and y(t) is carried out as

$$X(s) = L[x(t)], \quad Y(s) = L[y(t)]. \tag{2.2}$$

When the ratio to X(s) of Y(s) is taken, it is the function of s unrelated to the waveform and size of an input signal, and moreover, is a function peculiar to the circuit element. This function at the time of making all the initial values into zero is called transfer function.

$$H(s) = \frac{Y(s)}{X(s)}. \tag{2.3}$$

Composition of transfer functions

When two or more circuit elements are connected, a transfer function can be connected and it can be regarded as one circuit element.

1. series connection

$$H(s) = H_1(s)H_2(s). \tag{2.4}$$

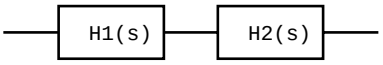

Figure 2.1: series connection

2. parallel connection

$$H(s) = H_1(s) + H_2(s). \tag{2.5}$$

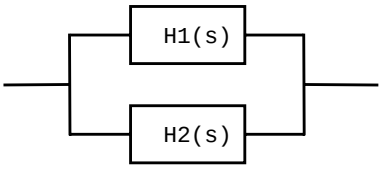

Figure 2.2: parallel connection

3. feedback connection

$$F(s) = \frac{G(s)}{1 \pm G(s)(Hs)}. \tag{2.6}$$

+:negative feedback -:positive feedback

frequency response

When sine wave is added to a linear element as an input signal, the output signal of a steady state is also sine wave of the same frequency. When considering the input signal of sine wave

$$x(t) = A_i \sin \omega t. \tag{2.7}$$

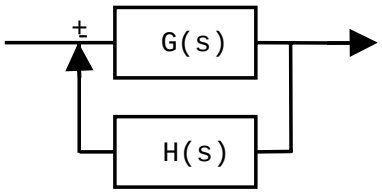

Figure 2.3: feedback connection

the output signal can be written as

$$y(t) = A_o \sin(\omega t + \phi). \tag{2.8}$$

The amplitude ratio $\frac{A_o}{A_i}$ is called gain, and phase difference ϕ is only called phase. When the frequency transfer function G($i\omega$) is defined as G(s) whose s is replaced with $i\omega$, gain and phase can be written down using G($i\omega$).

$$gain: \quad \frac{A_o}{A_i} = |G(i\omega)|. \tag{2.9}$$

$$phase: \quad \phi = \arg(G(i\omega)). \tag{2.10}$$

This is shown as follows.

Since Laplace transform of Eq. (2.7) is

$$X(s) = L[A_i \sin \omega t] = \frac{A_i \omega}{s^2 + \omega^2}. \tag{2.11}$$

Y(s) can be expressed as

$$Y(s) = G(s)X(s) = G(s)\frac{A_i \omega}{s^2 + \omega^2}. \tag{2.12}$$

As G(s) is a rational expression, it can be written as

$$G(s) = \frac{N(s)}{D(s)} = \frac{N(s)}{(s - s_1)(s - s_2)\cdots(s - s_n)}. \tag{2.13}$$

Using $s^2 + \omega^2 = (s - i\omega)(s + i\omega)$, Eq. (2.12) can be developed as

$$Y(s) = \frac{K_1}{s - s_1} + \frac{K_2}{s - s_2} + \cdots + \frac{K_n}{s - s_n} + \frac{K_+}{s - i\omega} + \frac{K_-}{s + i\omega}. \tag{2.14}$$

Performing inverse transform to this, we obtain

$$y(t) = K_1 e^{s_1 t} + K_2 e^{s_2 t} + \cdots + K_n e^{s_n t} + K_+ e^{i\omega} + K_- e^{-i\omega}. \tag{2.15}$$

In a steady state, the last two term remain.

$$y(t) = K_+ e^{i\omega} + K_- e^{-i\omega}. \tag{2.16}$$

K_+ and K_- are obtained as

$$K_+ = [Y(s) \cdot (s - i\omega)]_{s=i\omega} = \left[G(s) \frac{A_i \omega (s - i\omega)}{s^2 + \omega^2} \right]_{s=i\omega} = G(i\omega) \frac{A_i}{2i}. \tag{2.17}$$

$$K_- = [Y(s) \cdot (s + i\omega)]_{s=-i\omega} = \left[G(s) \frac{A_i \omega (s + i\omega)}{s^2 + \omega^2} \right]_{s=-i\omega} = G(-i\omega) \frac{A_i}{-2i}. \tag{2.18}$$

Here, $G(i\omega)$ is set with

$$G(i\omega) = |G(i\omega)| e^{i\theta}. \tag{2.19}$$

As $G(-i\omega)$ is a complex conjugate of $G(i\omega)$,

$$G(-i\omega) = |G(i\omega)| e^{-i\theta}. \tag{2.20}$$

Substituting these relations into Eq. (2.16), the output signal is expressed with $G(i\omega)$.

$$\begin{aligned} y(t) &= |G(i\omega)| \frac{A_i}{2i} (e^{i(\omega t + \theta)} - e^{-i(\omega t + \theta)}) && (2.21) \\ &= |G(i\omega)| A_i \sin(\omega t + \theta) && (2.22) \\ &= A_o \sin(\omega t + \phi). && (2.23) \end{aligned}$$

Thus, Eqs. (2.9) and (2.10) are obtained.

When $G(s)$ is known, we can know $G(i\omega)$ and frequency response of the system. G(s) is all the information we need to know about circuit elements.

2.1.2 Open loop transfer function

The role of the transfer function in a control system is considered here. First, open loop transfer function and closed loop transfer function in a control system are

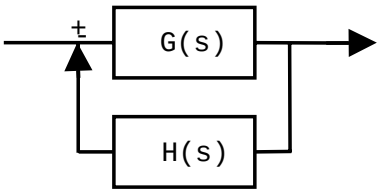

Figure 2.4: feedback system

defined. The general block diagram of a feedback control system becomes like Fig. 2.4

Open loop transfer function is defined as the product of the transfer function at the time of taking a round of a loop. In the case of Fig. 2.4, it is calculated as follows.

$$F_o(s) = G(s)H(s). \tag{2.24}$$

Closed loop transfer function is defined as the transfer function of the whole system. In the case of Fig. 2.4, it is calculated as follows.

$$F_c(s) = \frac{G(s)}{1 - G(s)H(s)}. \tag{2.25}$$

Using the closed loop transfer function F(s) and an input signal X(s), the output signal Y(s) can be written as follows.

$$Y(s) = F(s)X(s) = \frac{G(s)}{1 - G(s)H(s)}X(s). \tag{2.26}$$

Here, a signal is well controlled when $G(i\omega)H(i\omega)$ (open loop transfer function) is sufficiently larger than 1.

2.1.3 Stability condition

A control system may become unstable when delay is in the response of control. The condition for stable control system has many expressions. Here, we disscuss the stability condition only on Bode diagram.

The relation between a gain and frequency and the relation between a phase and frequency are expressed to a rectangular-coordinates system, respectively, and what was made into 1 set is called Bode diagram (Fig. 2.5).

The stable conditions are expressed with open loop transfer function $G(i\omega)$ as follows.

1. $|G(i\omega_p)| < 1, \quad at \;\; argG(i\omega_p) = -180$
2. $argG(i\omega_g) > -180, \quad at \;\; |G(i\omega_p)| = 1$

$|G(i\omega_p)|$ is called gain margin, and $argG(i\omega_g)$ is called phase margin.

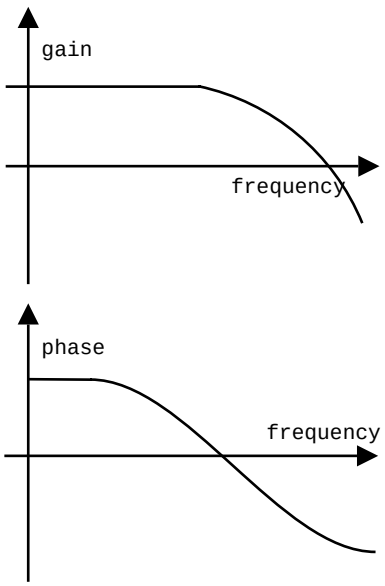

Figure 2.5: bode diagram

2.2 Optical system

Mach-Zehnder interferometer is composed of light source, detector, two mirrors and two half-silvered mirror (beamsplitter). The interferometer is shown on Fig. 2.6.

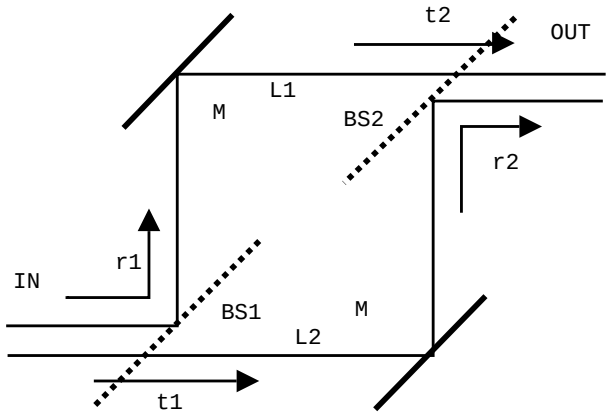

Figure 2.6: Mach-Zehnder interferometer

A light beam is first split into two parts by a beamsplitter and then recombined by a second beamsplitter. Depending on the relative phase acquired by the beam along the two paths, the intensity of output light differs.

Here, we consider the transmittance of Mach-Zehnder interferometer. t_1, t_2 are amplitude transmittance of half mirrors, and r_1, r_2 are amplitude reflectance of half mirrors. The electric field of the inputted light is written as

$$E_{in} = E_0 e^{i\omega}. \tag{2.27}$$

We set phases obtained in each path to ϕ_1 and ϕ_2. The electric field of the output light can be expressed as

$$E_{out} = t_1 r_2 E_0 e^{i(\omega t - \phi_1)} + t_2 r_1 E_0 e^{i(\omega t phi_2)}. \tag{2.28}$$

The power is written as follows.

$$\begin{aligned} P &= |E_{out}|^2 && (2.29)\\ &= |t_1 r_2 E_0 e^{i(\omega t - \phi_1)} + t_2 r_1 E_0 e^{i(\omega t - \phi_2)}|^2 && (2.30)\\ &= (t_1 r_2)^2 E_0^2 + (t_2 r_1)^2 E_0^2 + 2 t_1 t_2 r_1 r_2 E_0^2 \cos\Delta\phi && (2.31)\\ &= \frac{P_{max} + P_{min}}{2} + \frac{P_{max} - P_{min}}{2} \cos\Delta\phi. && (2.32) \end{aligned}$$

The transmittance is

$$\begin{aligned} T &= \frac{|E_{out}|^2}{E_0^2} && (2.33)\\ &= (t_1 r_2)^2 + (t_2 r_1)^2 + 2 t_1 t_2 r_1 r_2 \cos\Delta\phi && (2.34)\\ &= \frac{T_{max} + T_{min}}{2} + \frac{T_{max} - T_{min}}{2} \cos\Delta\phi. && (2.35) \end{aligned}$$

2.3 Data taking system

To detect $\Delta\phi$, we used modulation and demodulation of laser light. In this subsection, data taking system using modulation method is discribed.

2.3.1 Modulation

First, we modulated the intensity and frequency of laser light by passing small alternative current ($I_1 \cos\omega_m t$) through laser diode in addition to direct current (I_0). The total current (I) is

$$I = I_0 + I_1 \cos\omega_m t. \tag{2.36}$$

If frequency changes, since a phase will also change from the following relations, $\Delta\phi$ becomes a function of current I.

$$\Delta\phi = \frac{\omega\Delta L}{c}. \tag{2.37}$$

$$\Delta\phi = \Delta\phi(\omega) = \Delta\phi(I) = \Delta\phi(I_0 + I_1 \cos\omega_m t). \tag{2.38}$$

2.3.2 Demodulation

The information on a phase $\Delta\phi$ can be extracted by processing the output light of an interferometer by lock-in amplifier.

The signal inputted into a lock-in amplifier is multiplied by the reference signal similarly inputted from the outside, and is outputted through a low path filter. Simply, a lock-in amplifier consists of a multiplication circuit and a low pass filter, as shown in Fig. 2.7.

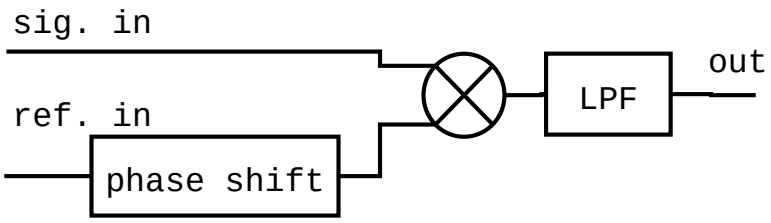

Figure 2.7: lock-in amplifier

Here, we consider the output signal of lock-in amplifier when modulated signal is inputted and sine wave is used as reference signal at the modulation frequency. A certain physical quantity A is regarded as a function of modulated quantity X. X can be expressed as a sum of constant X_0 and $x\cos\omega_m t$. ω_m is a modulation frequency. When x is sufficiently smaller than X, A is expressed as

$$A(X) = A(X_0) + \left.\frac{\partial A(X)}{\partial X}\right|_{X=X_0} x\cos\omega_m t. \tag{2.39}$$

In a lock-in amplifier, A(X) is multipled by reference signal $x\cos_m t$, and passes through a low pass filter. Only the clause proportional to $\cos_m t$ remains by these operations. Therefore, the output of lock-in amplifier becomes $\frac{\partial A(X_0)}{\partial X}$.

In the case of this experiment, A(X) is $\Delta\phi(I)$, and $X_0 + x\cos\omega_m t$ corresponds to $I_0 + I_1\cos\omega_m t$. The output is then

$$\left.\frac{\partial\Delta\phi(I)}{\partial I}\right|_{I=I_0} = \left.\frac{\partial}{\partial I} - (1+\cos\Delta\phi(I))\right|_{I=I_0} \tag{2.40}$$

$$= \sin\Delta\phi\left.\frac{\partial\Delta\phi(I)}{\partial I}\right|_{I=I_0}. \tag{2.41}$$

When $\left.\frac{\partial\Delta\phi(I)}{\partial I}\right|_{I=I_0}$ can be treated as a constant, the output of the lock-in amplifier is expressed as $C\sin\Delta\phi$ where C is a constant. Thus, the information on $\Delta\phi$ can be extracted using technique of modulation and demodulation.

2.4 Feedback system

In accordance with an optical system and a control system, a whole system as shown in Fig. 2.8 is constituted. Below, each loop of feedback is explained.

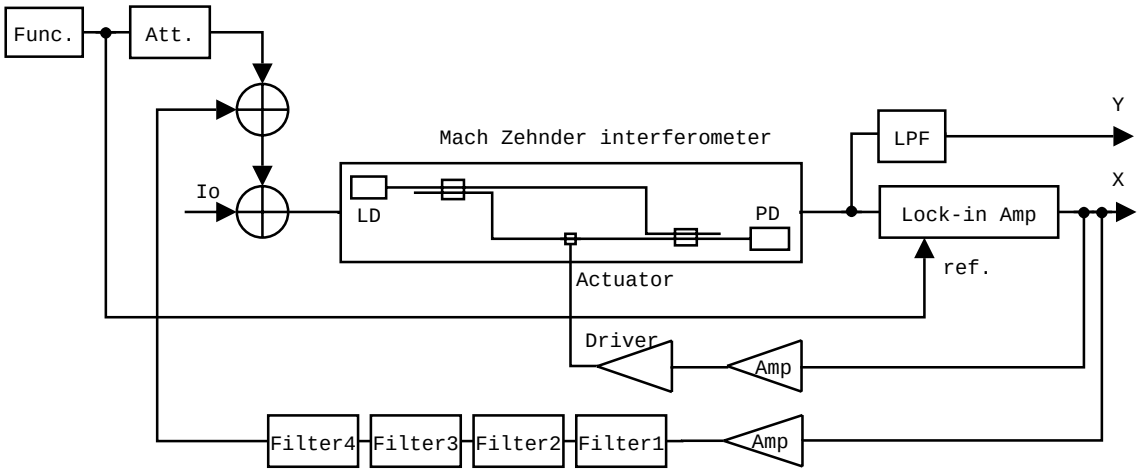

Figure 2.8: the whole feedback system

2.4.1 Laser frequency feedback

Since $\Delta\phi$ is related to ω by Eq. (2.42), we can stabilize laser frequency by fixing $\Delta\phi$ to a certain value.

$$\Delta\phi = \frac{\omega\Delta L}{c}. \tag{2.42}$$

As seen in the previous subsection, the output signal of lock-in amplifier is proportinal to $\sin\Delta\phi$. Laser intensity is changed by carrying out the negative feedback of this quantity at LD current. Since the intensity of laser is closely related to frequency, thereby, frequency also changes. Thus, frequency can be controlled near the value where

$$\sin\Delta\phi = \sin\frac{\omega\Delta L}{c} = 0 \tag{2.43}$$

is realized.

A block diagram for this loop is shown in Fig. 2.9. Open loop transfer function is

$$F_o(s) = G_1G_2H_1. \tag{2.44}$$

and closed loop transfer function is

$$F_c(s) = \frac{G_1G_2}{1 + G_1G_2H_1}. \tag{2.45}$$

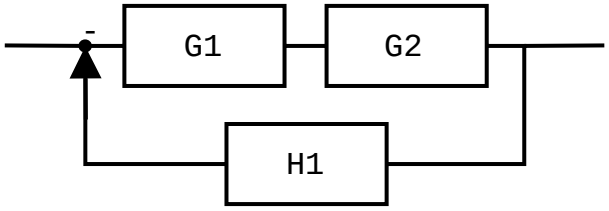

Figure 2.9: block diagram of laser loop feedback system

2.4.2 Light path feedback

In the relation Eq. (2.42), ΔL must be stable in order to determine ω with sufficient accuracy. However, an optical fiber is expanded and contracted with temperature at low frequency. In order to suppress these expansion and contraction, we controlled the length of an optical fiber using Peltier element. Current flows in Peltier element according to the output of lock-in amplifier $\sin\Delta\phi$. In other words, ΔL is controlled instead of ω. This loop itself cannot stabilize the laser frequency, but it stabilize ΔL and make it possible at high frequency for another loop.

A block diagram for this loop is shown in Fig. 2.10. Open loop transfer function is

$$F_o(s) = G_2H_2. \tag{2.46}$$

and closed loop transfer function is

$$F_c(s) = \frac{G_1 G_2}{1 + G_2 H_2}. \tag{2.47}$$

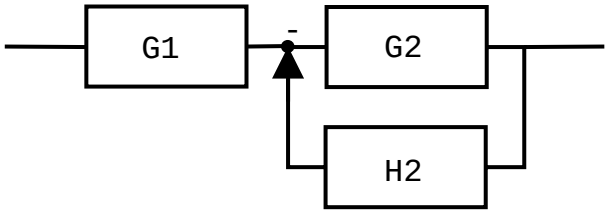

Figure 2.10: block diagram of Peltier loop feedback system

2.4.3 2-loop control

Because of the relation below, ω can be stabilized by fixing $\Delta\phi$ and ΔL.

$$\Delta\phi = \frac{\omega \Delta L}{c}. \tag{2.48}$$

This can be realized by 2 loops descrived above.

A block diagram for this loop is shown in Fig. 2.11. Open loop transfer function is

$$F_o(s) = G_2 H_2 + G_2 G_1 H_1. \tag{2.49}$$

and closed loop transfer function is

$$F_c(s) = \frac{G_1 G_2}{1 + G_2 H_2 + G_2 G_1 H_1}. \tag{2.50}$$

Open loop transfer functions for (i)1-loop(Laser loop), (ii)1-loop(Peltier loop) (iii)2-loop are called $G_l, G_p, G_l p$ below.

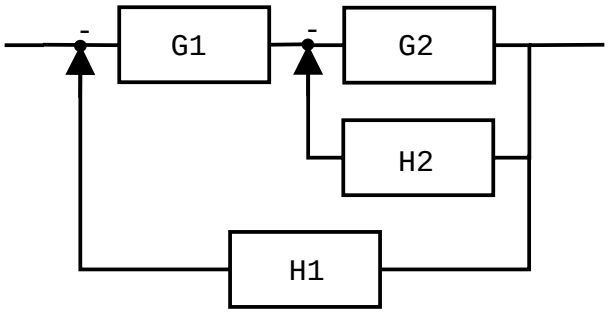

Figure 2.11: block diagram of 2-loop feedback system

Chapter 3

Experiment and results

3.1 Optical system

3.1.1 Characteristics of Laser diode

We measured current characteristic and temperature characteristic of laser diode with a system shown in Fig. 3.1.

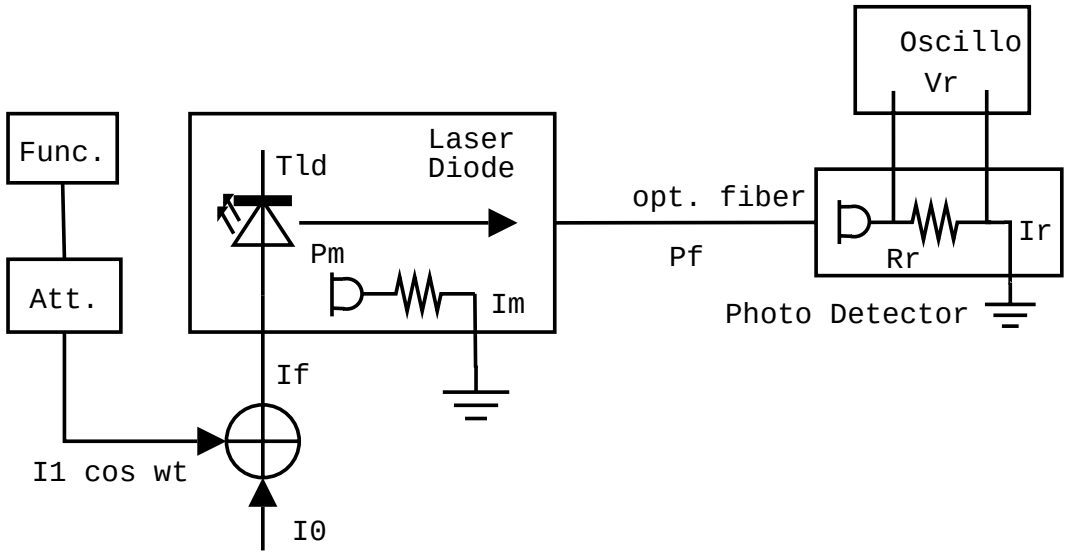

Figure 3.1: optical system

The LD driver controls I_f, the LD current. The temperature controller regulates T_{LD}, the temperature of LD. The photo diode of a built-in formula is near the diode, and the output current I_m can be checked with a driver. 100 μA of I_m is equivalent to 10 mW of the power P_m. P_f is the power of laser light which conducts through the optical fiber. Another photo detector is at the other end of the fiber. I_r is the

output current of this photo diode. The output of the photo detector measured with oscilloscope is V_r, which is the product of I_r and resistance R_r. R_r is usually set to 1kΩ.

current sharacteristic

First, the relation between I_f, P_m and V_r is measured. The results are shown in Fig. 3.2, Fig. 3.3, and Fig. 3.4.

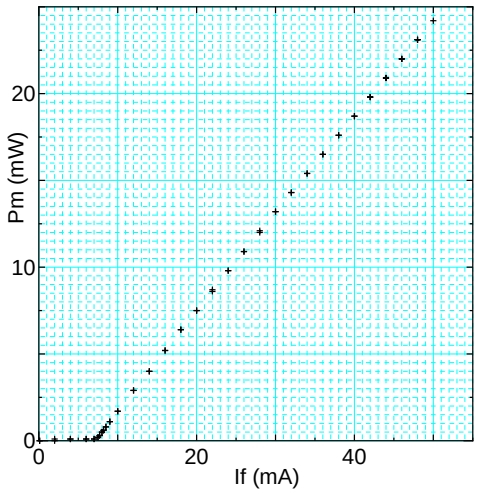

Figure 3.2: LD characteristic (If-Pm)

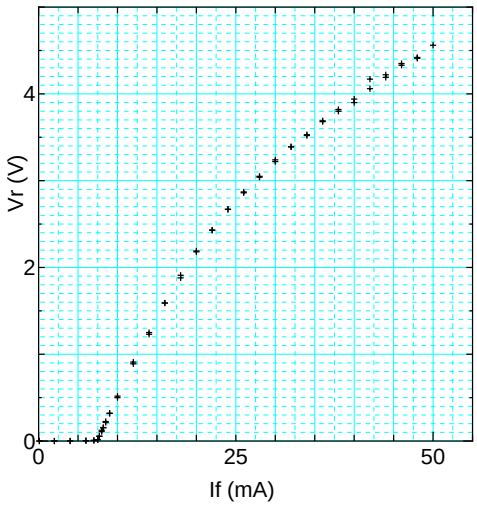

Figure 3.3: LD characteristic (If-Vr)

When I_f is large, the relation between I_f and V_r is not linear. This is thought of because photo diode is saturated when inputted light is intense. However, this is not important as the photo diode is used in the area P_m is smaller than 5mW in the following experiment.

temperature characteristic

Next, we measured the relation between T_{LD} and V_r. The result is shown in Fig. 3.5.

This figure shows that the output power of laser diode decreases when the temperature increases, and that the relation is linear.

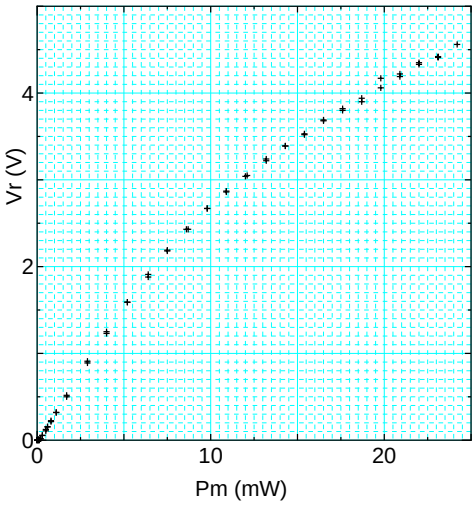

Figure 3.4: LD characteristic (Pm-Vr)

3.1.2 Splitting ratio of beam splitter

The branch ratio of the beam splitter which is one of the important composition elements of an optical system was measured. A beam splitter has the input of two fibers A and B, and the output of two fibers X and Y, there being also a contrary (Fig. 3.6).

First, we measured the output light intensity of fiber X when laser light is inputted to fiber A (shown in Fig. 3.7). This splitter is used in order to unite the mode of laser light with the fiber used for a splitter. That is, the characteristics of another beam splitter is measured regarding the group of laser and one splitter as a light source. The result is shown in Table. 3.1.

I_f (mA)	V_r (mV)
10	33.0
15	102.0

Table 3.1: output of BS1 (A-X)

Next, another beam splitter (BS2) is connected to fiber X of BS1 (shown in Fig. 3.8). BS2 is connected in four ways (A-X, A-Y, B-X, and B-Y), and the output light intensity is measured about each case. The result is shown in Table. 3.2.

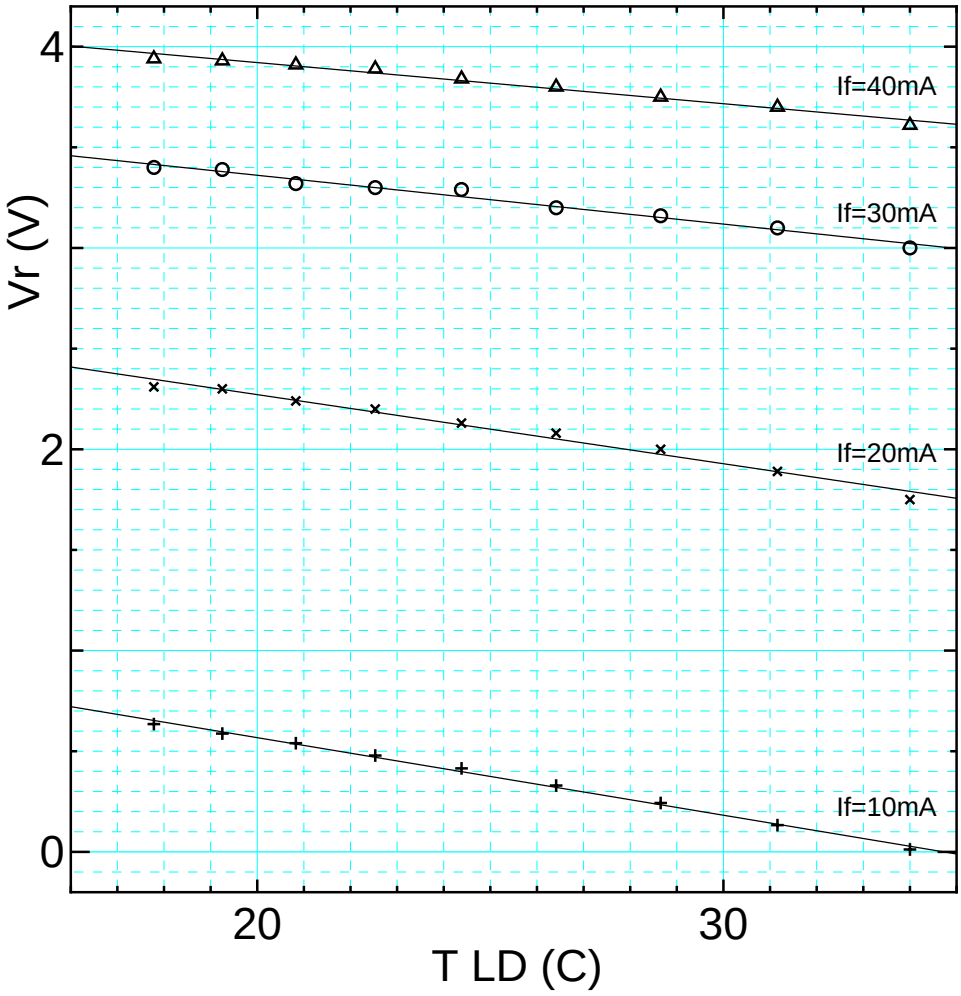

Figure 3.5: temperature characteristic laser diode

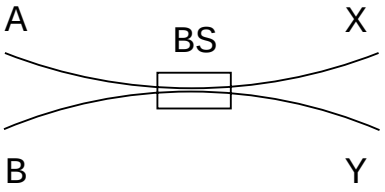

Figure 3.6: beam splitter

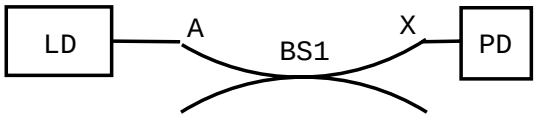

Figure 3.7: mode matching of laser light

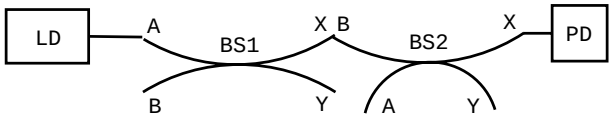

Figure 3.8: measurement of branch ratio

Since the branch ratio is about 1:1, it turns out that this beam splitter can be used to make the interferometer of high contrast.

3.1.3 Mach-Zehnder interferometer

Mach-Zehnder interferometer is a interferometer using two mirrors and two half mirrors as shown in Fig. 2.6. We constructed this interferometer with fiber laser and two beam splitters. The optical system consists of an interferometer, fiber laser, a photo detector, and an oscilloscope, which is shown in Fig. 3.9.

The output of the interferometer is measured with oscilloscope, which is expressed as follows.

$$P = \frac{P_{max} + P_{min}}{2} + \frac{P_{max} - P_{min}}{2} \cos \Delta\phi. \tag{3.1}$$

We measured P_{max} and P_{min} for four combinations of two beam splitter. Combinations are expressed as A-(X,Y)-(B,A)-X for example, which means that laser light is inputted to fiber A of BS1, splitted to two paths A-X-B-X and A-Y-A-X.

I_f (mA)	10		15	
	V_r (mV)	branch ratio	V_r (mV)	branch ratio
BS1(A-X) BS2(A-X)	17.3	0.52	54.0	0.53
BS1(A-X) BS2(A-Y)	15.4	0.47	48.1	0.47
BS1(A-X) BS2(B-X)	15.5	0.47	50.1	0.49
BS1(A-X) BS2(B-Y)	14.9	0.45	46.7	0.46

Table 3.2: branch ratio

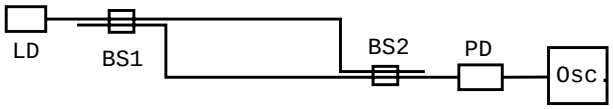

Figure 3.9: Mach-Zehnder interferometer

The results are shown below.

	P_{max} (mV)	P_{min} (mV)	C
A-(X,Y)-(A,B)-X	580	14	0.95
A-(X,Y)-(B,A)-X	590	4.5	0.99
A-(X,Y)-(A,B)-Y	560	6.5	0.98
A-(X,Y)-(B,A)-Y	560	1.5	1.00

Table 3.3: Contrust of the interferometer

Here, the contrust C is defined as

$$C = \frac{P_{max} - P_{min}}{P_{max} + P_{min}}. \tag{3.2}$$

The clarity of an interferometer is expressed with this value.

3.2 Data taking system

3.2.1 Modulation

We modulated the intensity and frequency of laser light by passing small alternative current ($I_1 \cos \omega_m t$) through laser diode in addition to direct current (I_0). First, the intensity dependability and frequency dependability of modulation were investigated using the optical system shown in Fig. 3.10. A function generator is used to generate the alternative current $I_1 \cos \omega_m t$.

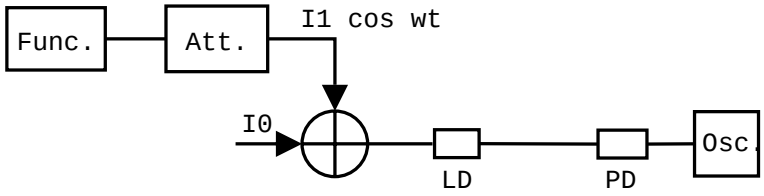

Figure 3.10: modulation

The frequency is set to 0.01Hz or 20kHz, and the direct current I_0 is 15mA or 40mA. The amplitude of the alternative current I_1 is set to 4mA or 1mA. The maximum and minimum value of output V_r can be estimated using the relation between I_f and V_r shown in Fig. 3.3. The results are shown in Table.3.4. The estimated V_r is written as V_r^{est}.

f (Hz)	I_0 (mA)	I_1 (mA)	V_r max (V)	V_r min (V)	V_r^{est} max (V)	V_r^{est} min (V)
0.01	15	4	2.1	0.7	2.1	0.7
	40	4	4.2	3.7	4.2	3.7
20000	15	1	1.46	1.14	1.46	1.16
	40	1	3.92	3.80	3.89	3.79

Table 3.4: intensity and frequency dependence of modulation

Coincidence of a result and an estimated values shows that laser modulation is successful regardless of intensity and frequency. We adopted 20kHz as f, and 1mA as I_1 in the experiment below.

3.2.2 Demodulation

The system is composed using a function generator for modulation, a laser driver, a laser diode, a Mach-Zehnder interferometer, a photo detector, lock-in amplifier for demodulation, and an oscilloscope. The output signal of the lock-in amplifier is inputted to X terminal of the oscilloscope, and the output signal of the photo detector is inputted to Y terminal.

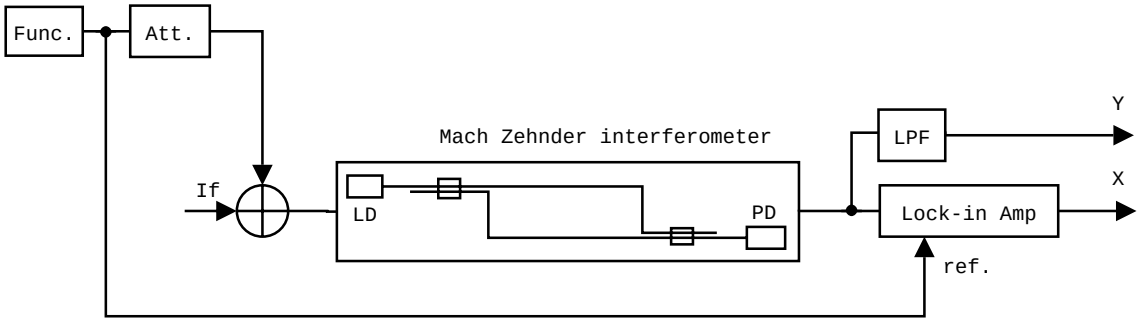

Figure 3.11: demodulation

As is seen in section 2.3.2, the inputted signals are expressed as

$$X = B \sin \Delta\phi. \tag{3.3}$$

$$Y = -A(1 + \cos\Delta\phi). \tag{3.4}$$

When taking account of the construst of the interferometer C,

$$Y = -A(\frac{1}{C} + \cos\Delta\phi). \tag{3.5}$$

Then, the locus of (X,Y) draws

$$\left(\frac{X}{B}\right)^2 + \left(\frac{1}{C} + \frac{Y}{A}\right)^2 = 1. \tag{3.6}$$

It becomes an eclipse on a display of the oscilloscope as shown in Fig. 3.12.

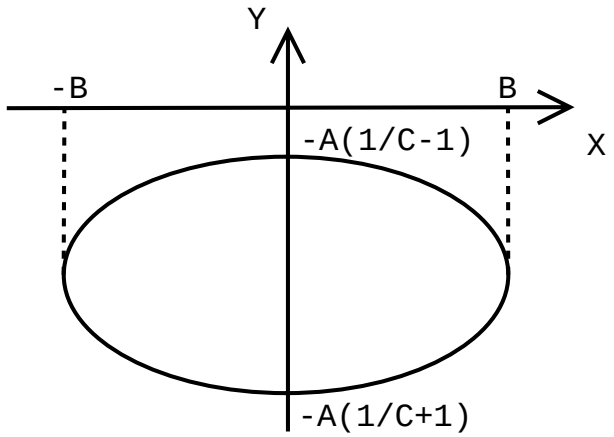

Figure 3.12: X-Y display on oscilloscope

By adjusting a phase of lock-in amplifier, we obtained a locus shown in Fig. 3.13 in the end. The contrust is

$$C = \frac{245 - 5}{245 + 5} = 0.96, \tag{3.7}$$

which is not contradictory to the result in section 3.1.3.

3.3 Feedback system

Laser frequency is stabilized by feedback to laser current and Peltier element. The former feedback controls the laser frequency, whild the latter controls the length of the optical path. In this section, these feedback loops are discribed.

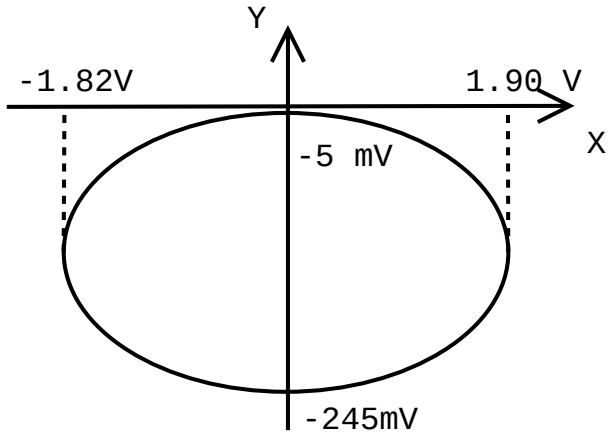

Figure 3.13: X-Y display on oscilloscope

3.3.1 Laser current feedback

First, we tried P(proportional) control of laser current. Since the laser current is closely related to the laser frequency, it means to control the laser frequency as well. The system below was composed.

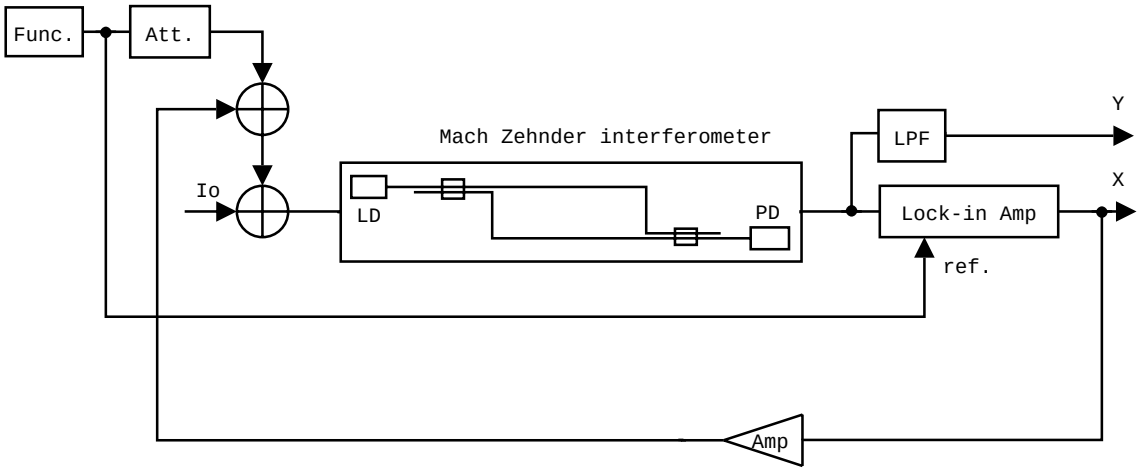

Figure 3.14: Laser current feedback

Since the error signal is the output of the lock-in amplifier $\sin\Delta\phi$, $\sin\Delta\phi$ is to be locked at 0, point A shown in Fig. 3.15.

Although the gain of amplifier was adjusted, stable control was not realized by this control system. However, signs that it was controlled were found near point A.

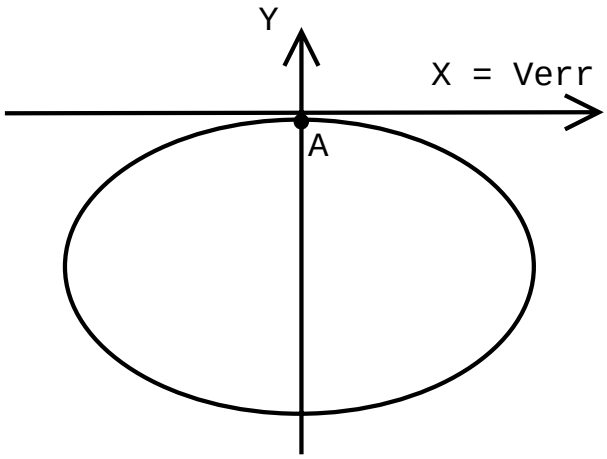

Figure 3.15: lock of $\Delta\phi$

The cause of the instability is thought to be as follows. That is, optical fiber expands and contrasts because of the fluctuation of temperature. Thus, the phase also flucutuate widely in low frequency. Two solutions can be considered against this problem. First, it is expected that PID control of laser current would be effective. The other solution is to control the length of the optical path to supress the influence of temperature. These trials are described in the following subsections.

3.3.2 PID control

In this subsection, PID control of laser current is described. The filter with the frequency characteristic as shown in Fig. 3.16 was created. This filter is called Filter1 below.

Lifting of the gain in low frequency corresponds to I(integral) control, and lifting of the gain in high frequency corresponds to D(differential) control. The gain in low frequency is increased by I control, and the phase margin is improved by D control. Filter1 was added to the system as shown in Fig. 3.17.

By adjusting the gain of amplifier, we have succeeded in $\Delta\phi$ fixation. The effectiveness of PID control was proved by this result.

3.3.3 Peltier feedback

The control of the length of an optical path was also tried. The fiber of one optical path was attached to the surface of a Peltier element as shown below. In order to raise the heat conductivity, optical grease was applied on the surface of the element.

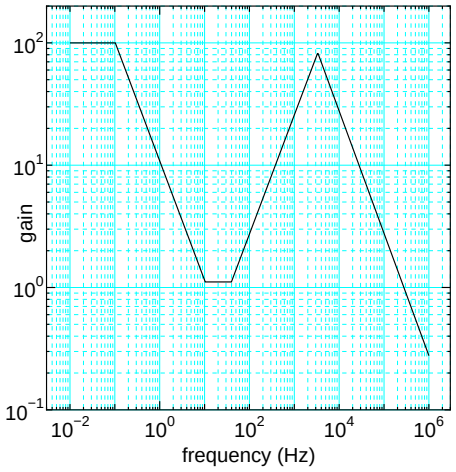

Figure 3.16: frewuency characteristics of Filter1

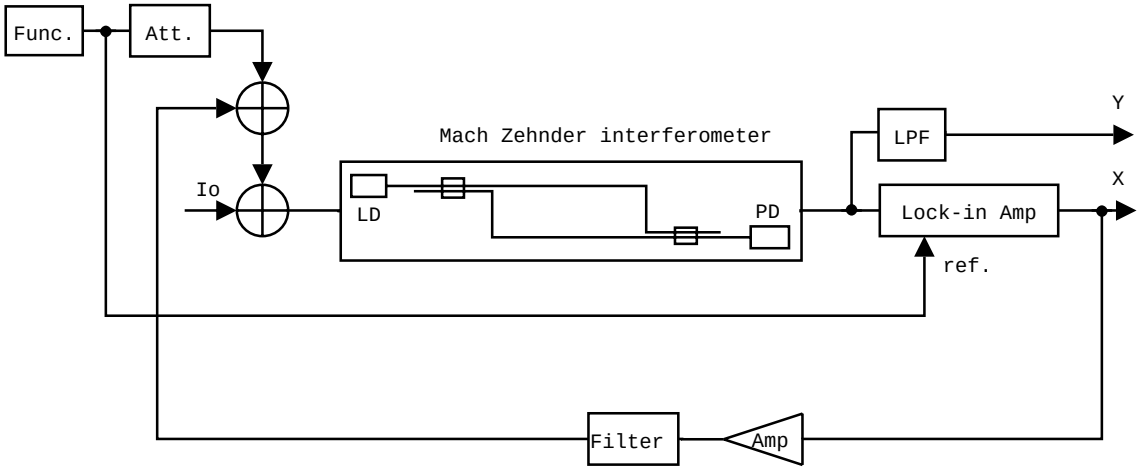

Figure 3.17: PID control

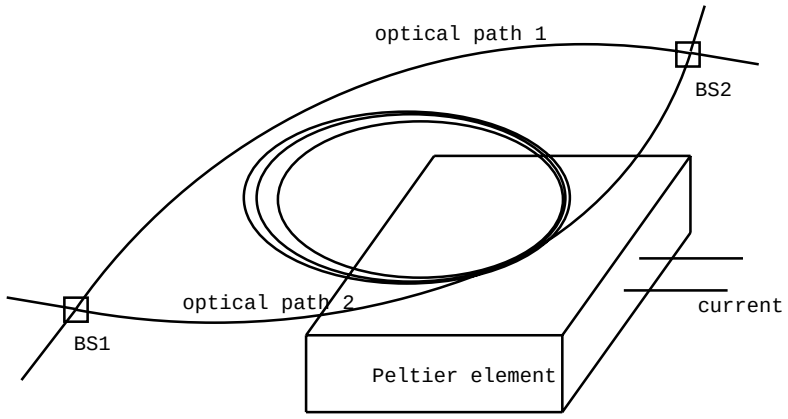

Figure 3.18: attachement of a fiber to Peltier element

The feedback system was composed using Peltier element (Fig. 3.19).

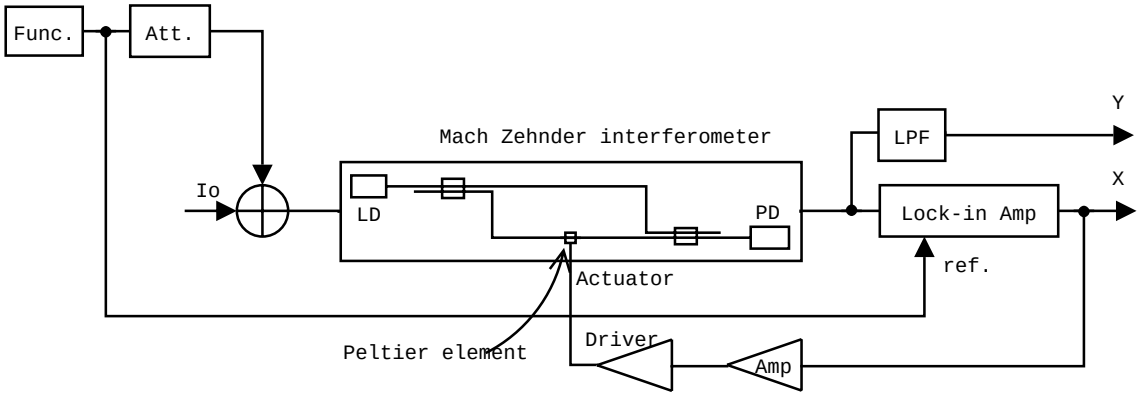

Figure 3.19: Peltier feedback

By adjusting the gain of amplifier, we have succeeded in control of optical path difference and $\Delta\phi$ was locked.

3.3.4 2-loop feedback

In response to the success of PID control and optical length control, we decided to perform these control simultaneously further. We constituted 2-loop feedback system from combination of laser loop and peltier loop (Fig. 3.20).

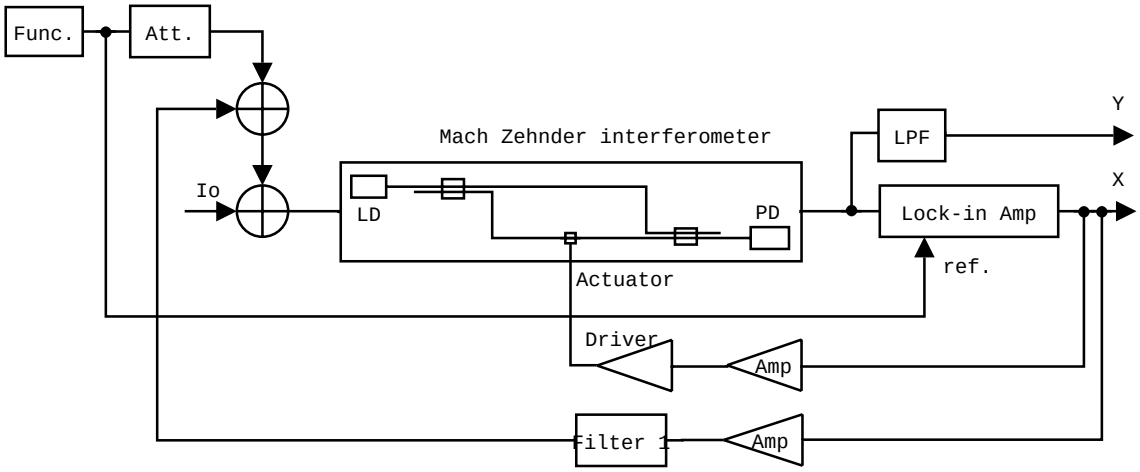

Figure 3.20: 2-loop feedback

By adjusting the gain of amplifiers, we have succeeded in control of $\Delta\phi$. The behavior of the point on an ascilloscope display indicates the improvement of control compared with that of 1-loop feedback. In the following subsection, this sign is confirmed numerically.

3.3.5 Evaluation of stability

Here, stability of a control system is evaluated. 2-loop control is compared with 1-loop(Peltier loop) control since laser loop is the only loop that stabilize the laser frequency.

First, open loop transfer function was measured in the cases of 2-loop and Peltier loop. Open loop transfer function can be measured using a spectrum analyzer (Fig. 3.21).

The results are shown in Fig. 3.22-3.23. Fig. 3.22 shows that the laser frequency can be stabilized from 2Hz to 400Hz where $|Glp| > 1$. A depression of Glp at 1.5Hz originates in the difference in phase between Gp and Gl. It can make the system unstable that $|Glp|$ is close to 1 because of the depression.

Measurement of power spectrum

The stability of a control system can be expressed as the fall in a power spectrum.

S_P, power spectrum in the case of Peltier loop control is expressed with S_0, the

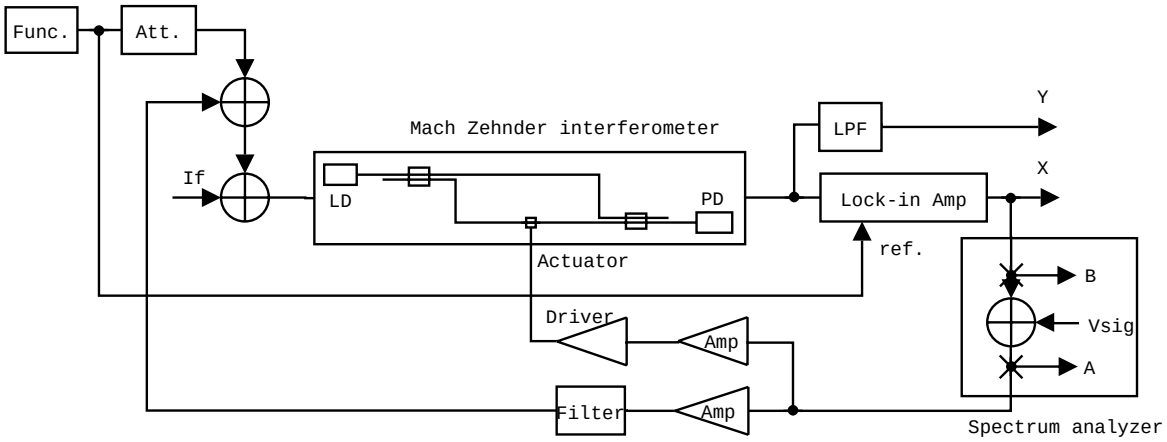

Figure 3.21: measurement of open loop transfer function

power spectrum in the case no control has been performed.

$$S_P = \frac{1}{|1 + G_P|} S_0. \tag{3.8}$$

S_{LP} can also be expressed as

$$S_{LP} = \frac{1}{|1 + G_{LP}|} S_0. \tag{3.9}$$

Therefore, the relation between S_{LP} and S_P is written as

$$S_{LP} = \frac{|1 + G_P|}{|1 + G_{LP}|} S_P. \tag{3.10}$$

Because of this relation, we can calculate the theoretical curve of S_{LP}. This theoretical curve is set to S_{LP}^{th}.

Power spectrum was measured in the cases of 2-loop and Peltier loop. Open loop transfer function can be measured using a spectrum analyzer (Fig. 3.24).

The results are shown in Fig. 3.25. S_{LP}^{th} was calculated using the relation Eq. (3.10). S_{LP} is consistent with S_{LP}^{th} from 10 to 400Hz. The reason of the disagreement from 1 to 10Hz might be an influence of exterior disturbance, but it is not clear. Setting this disagreement aside, the results in Fig. 3.25 shows that the stabilization of laser freequency was successful.

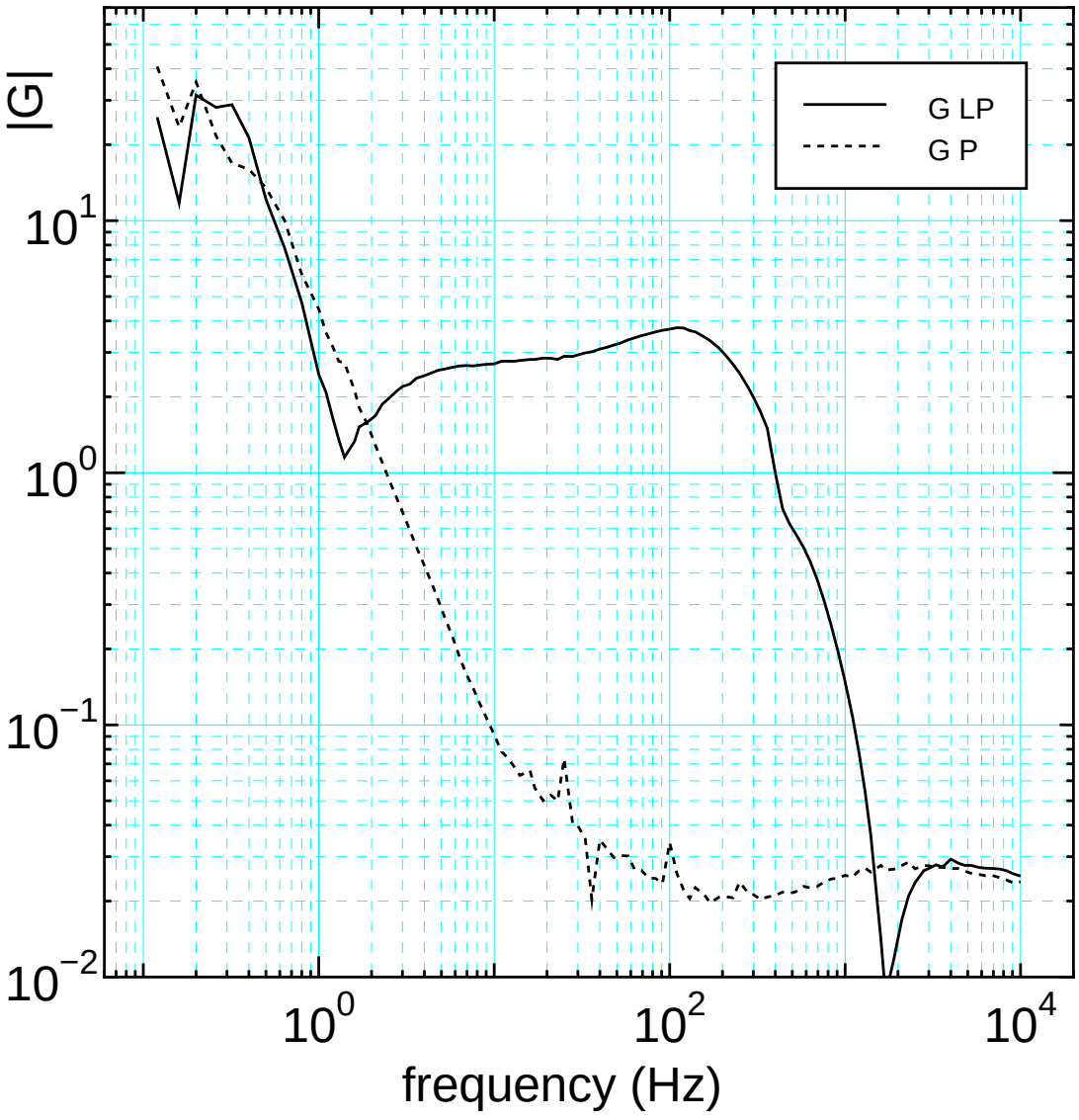

Figure 3.22: open loop transfer function

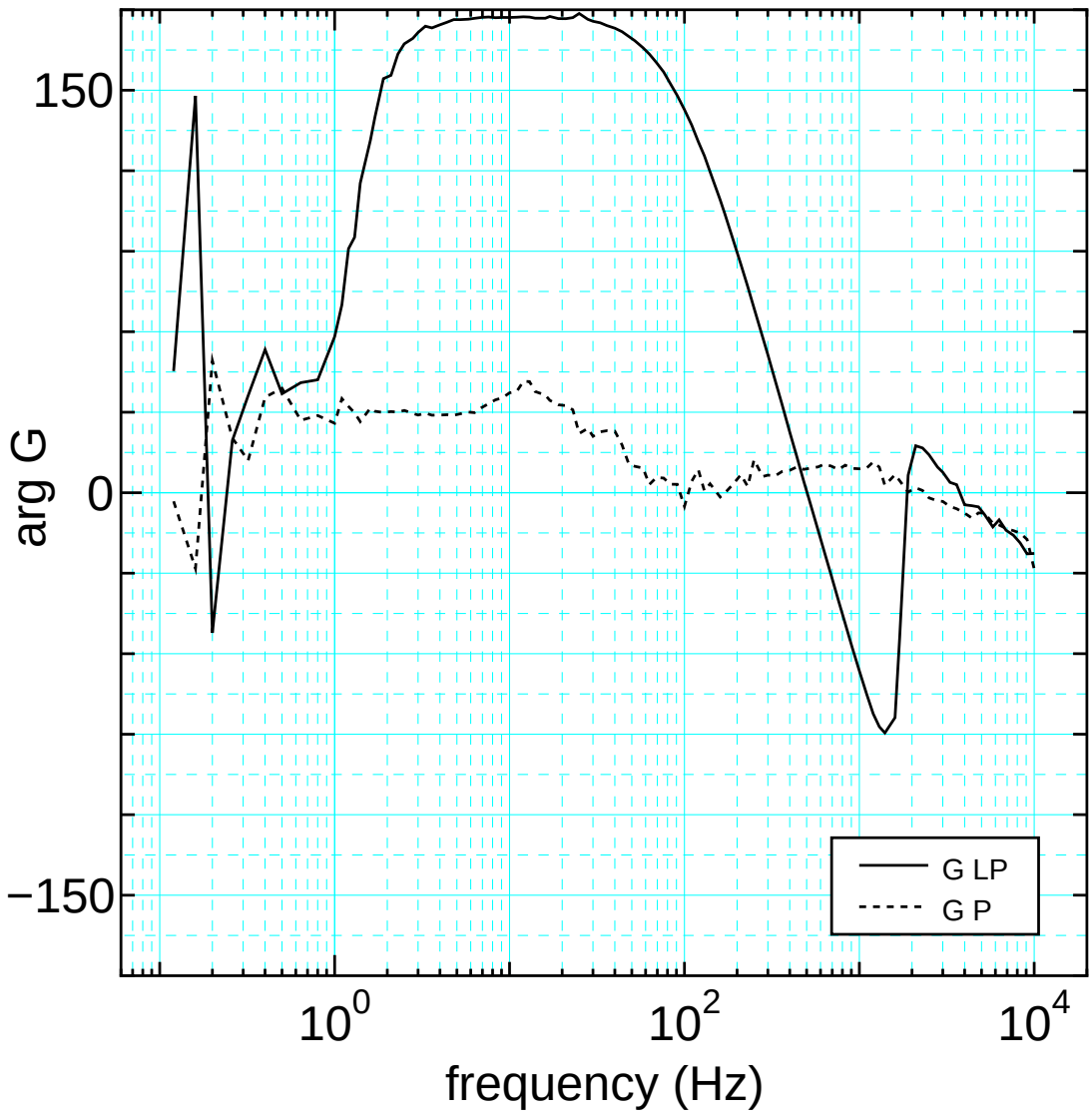

Figure 3.23: open loop transfer function

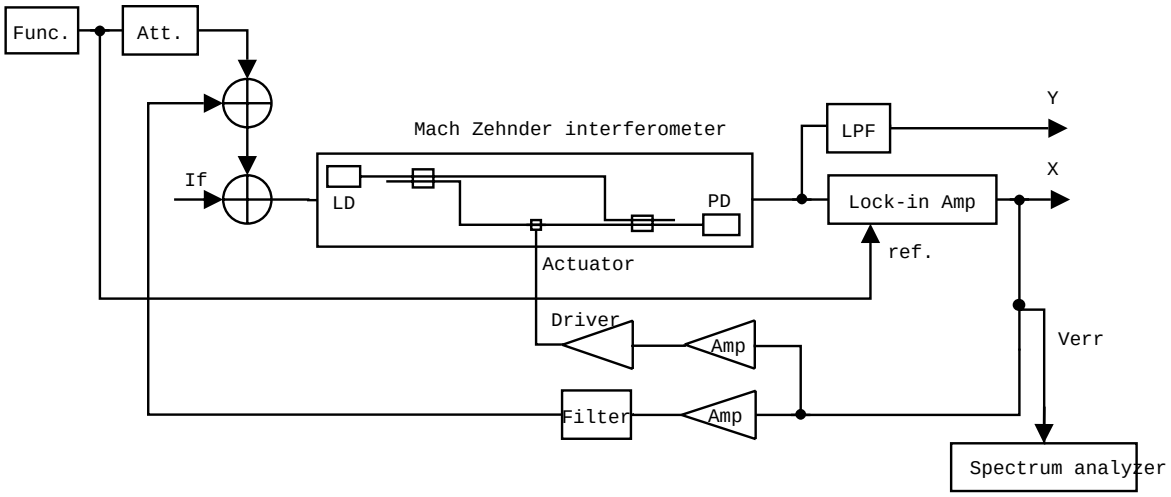

Figure 3.24: measurement of power spectrum

3.3.6 Improvement in stability

The stabilization of the laser frequency have succeeded with the system in the previous section. Here, improvement in the stability and the further capability of the system was tried.

The instability can be caused by the depression of *Glp* at 1.5Hz. We made two filters (Filter2 and Filter3) to raise *Glp* in low frequency. Fiter2 and Filter3 were made so that the gain is variable. Filter3 was made so that the time constant is also variable. Filter4 was made to drop the gain of laser loop to 0 in very low frequency. The frequency characteristic of each filter is shown in Fig. 3.26-3.28.

We tried various parameters of filters and it was made for the frequency characteristic of the gain of a circuit element which put all the filters in order to become as for it to be shown in Fig. 3.29. Adding these filters to the system, it was composed as shown in Fig. 3.30.

In this system, G_P, G_{LP}, S_P, S_{LP}, and S_{LP}^{th} were measured. The results are shown in Fig. 3.31-3.33. Fig. 3.33 shows that the stabilization of laser frequency was successful from under 1Hz to 300Hz.

As a comparison with Fig. 3.25, the result is improved in two points. First, the depression of G_{LP} has dissappeared. This is thought to be because the frequency where G_P and G_L crosses is off to the lower side, though it was unable to measure G_{LP} in lower frequency than 1Hz with a spectrum analyzer.

The other improvement is the stability of the system. The maximum fall of

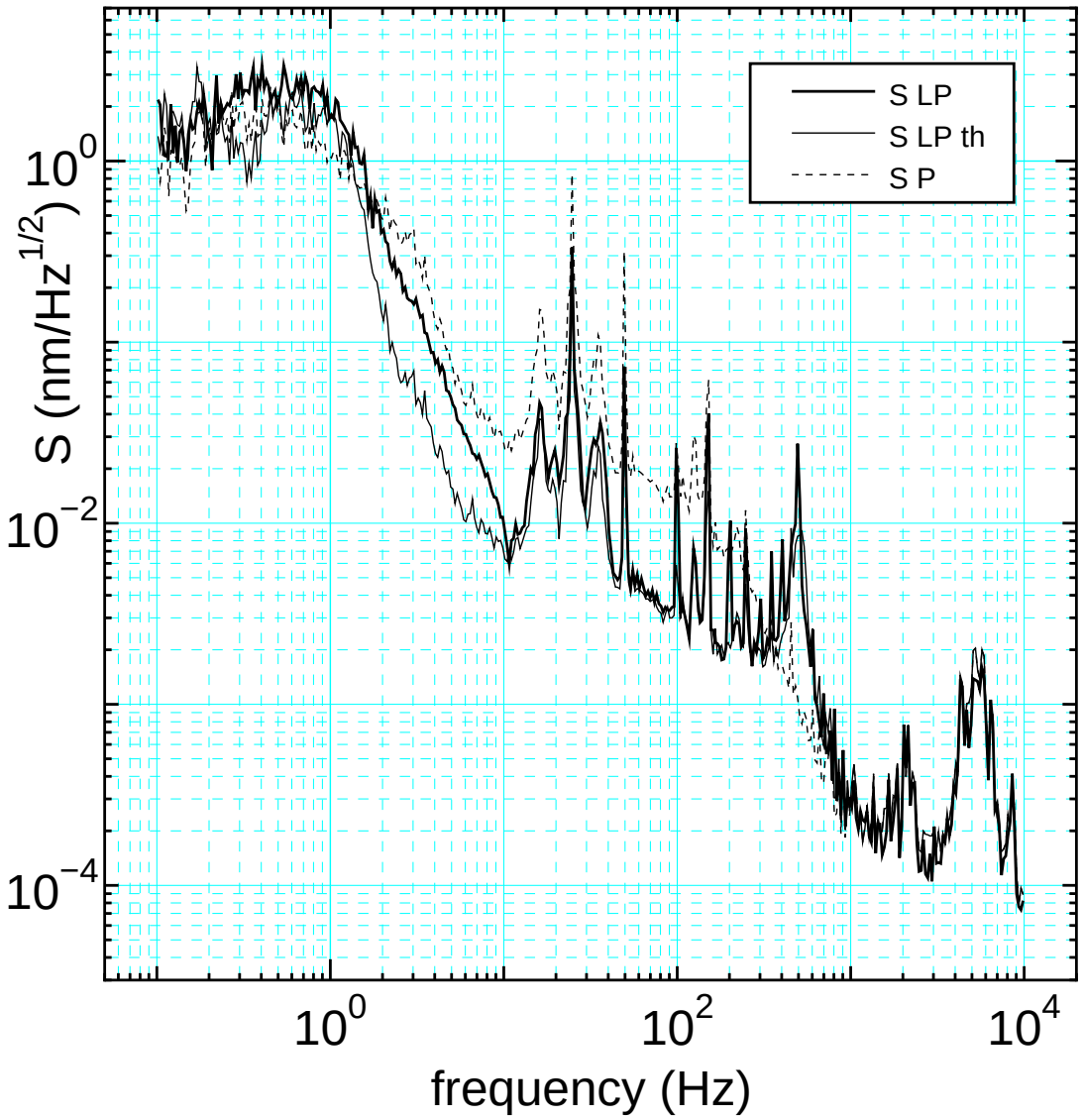

Figure 3.25: power spectrum

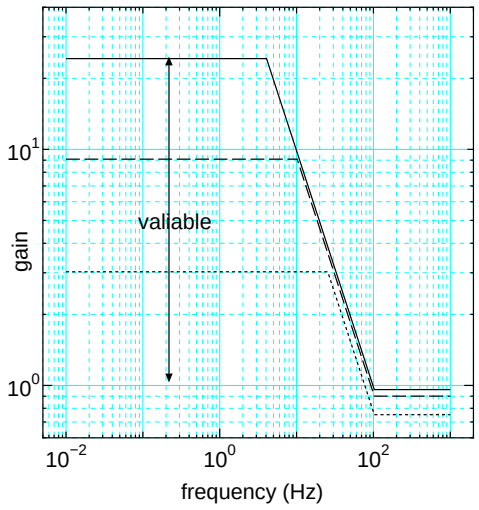

Figure 3.26: freqency characteristic of Filter2

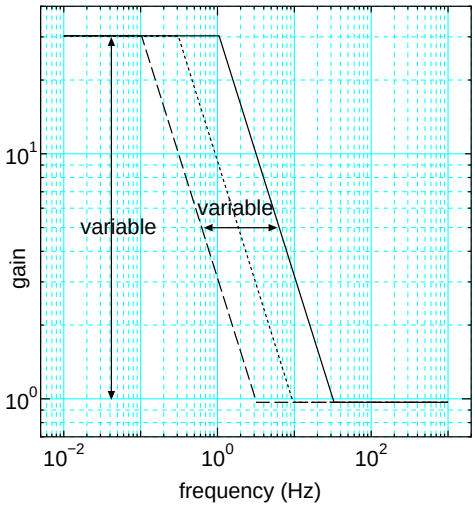

Figure 3.27: freq. char. of Filter3

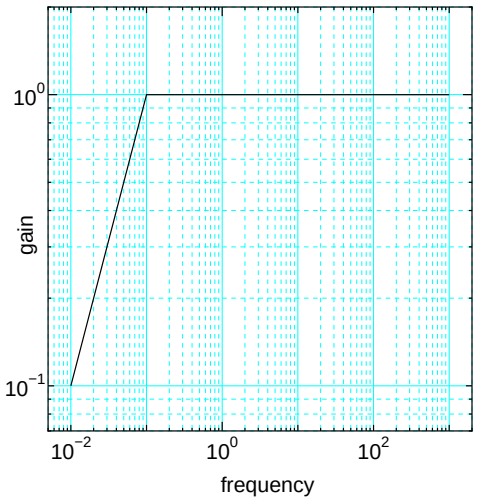

Figure 3.28: freq. char. of Filter4

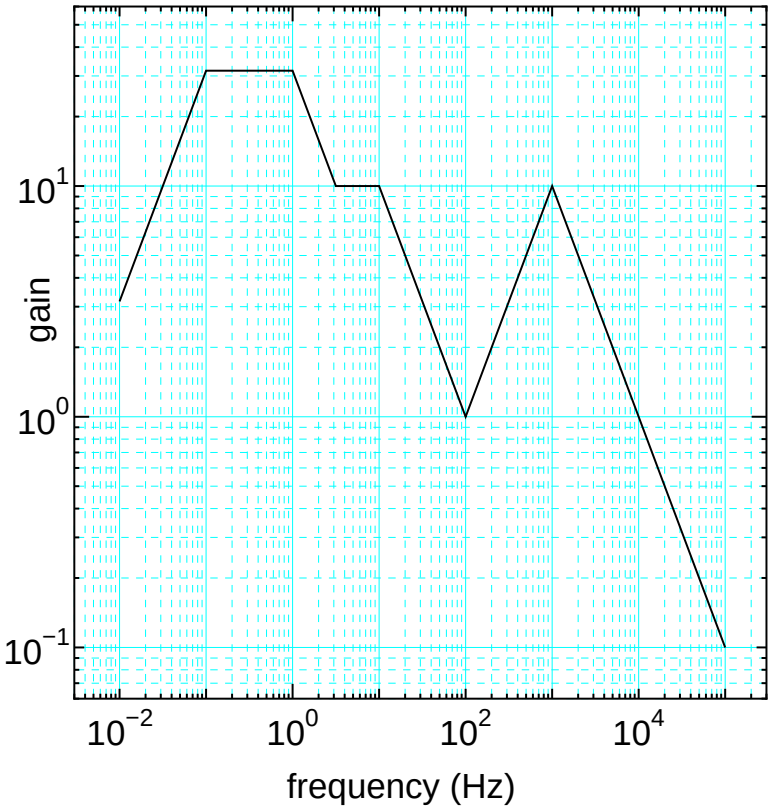

Figure 3.29: frequency characteristic of Filter1-4

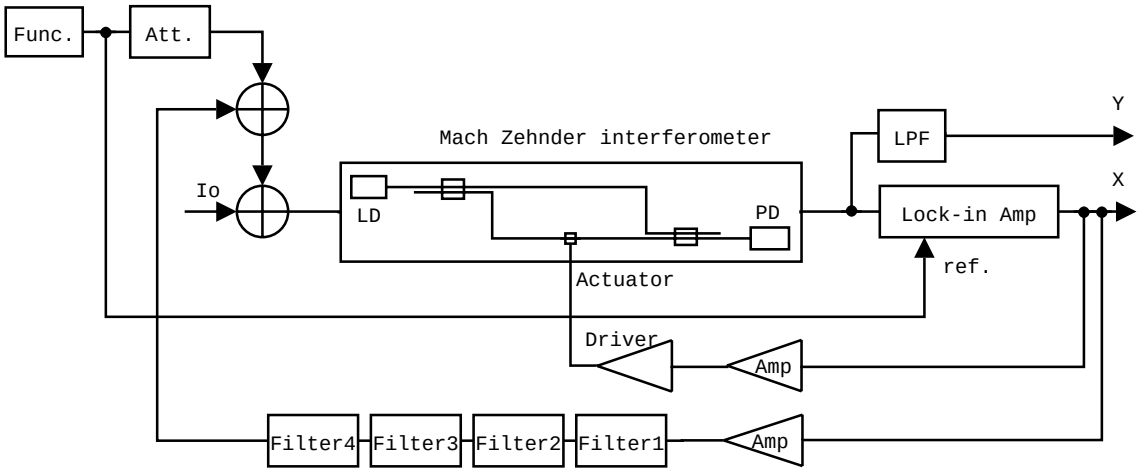

Figure 3.30: 2-loop control with Filter1-4

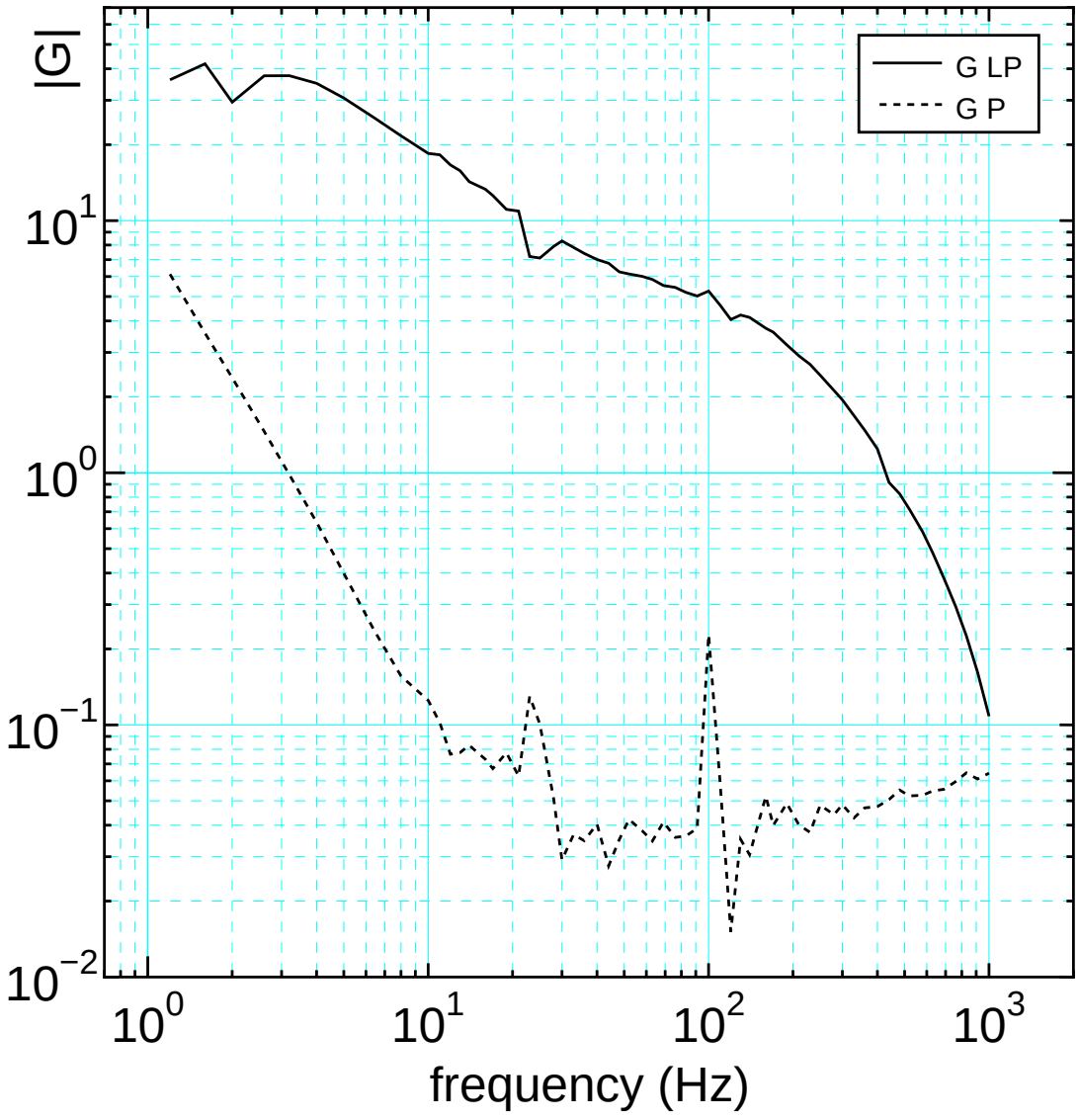

Figure 3.31: open loop transfer function

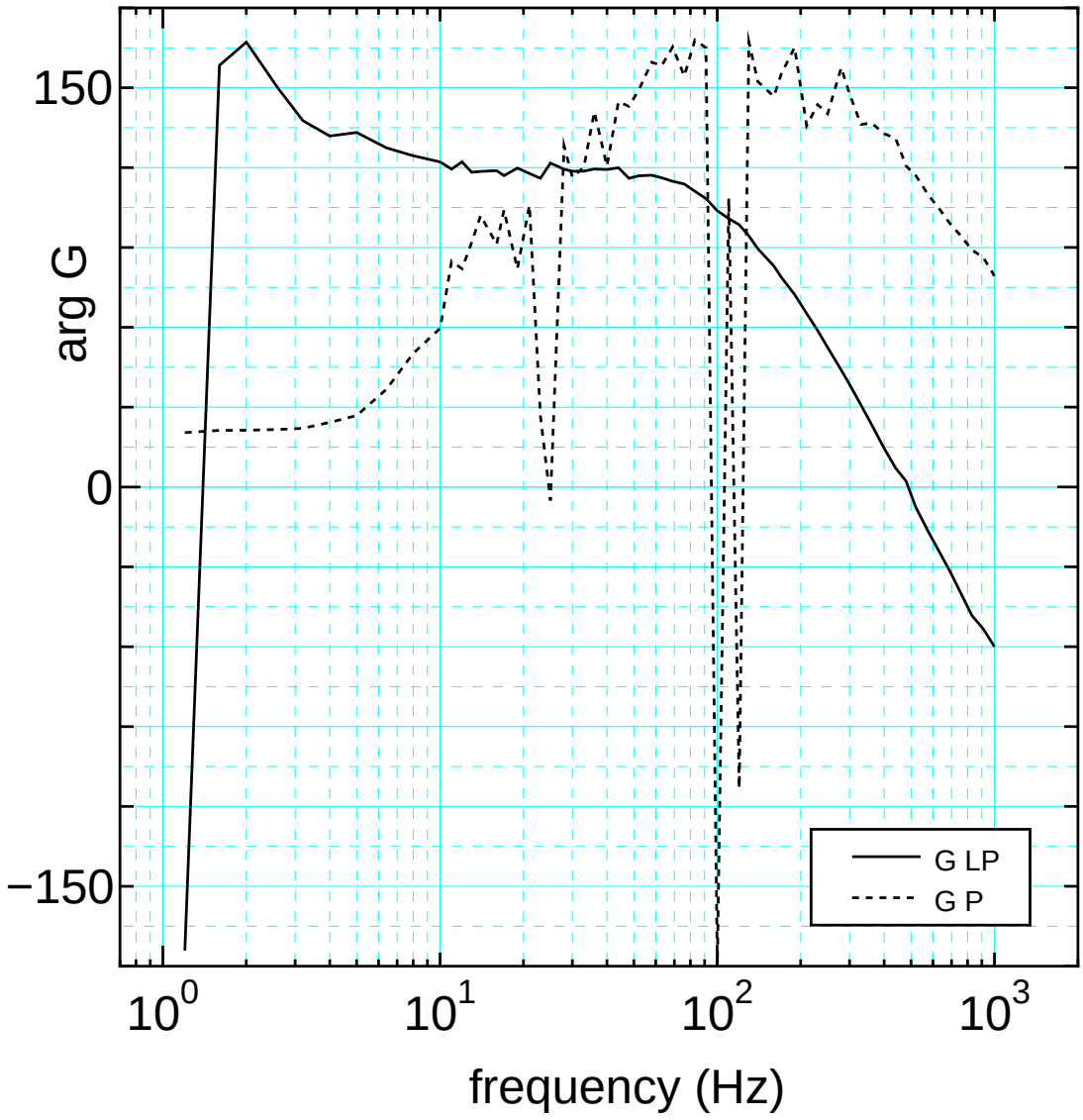

Figure 3.32: open loop transfer function

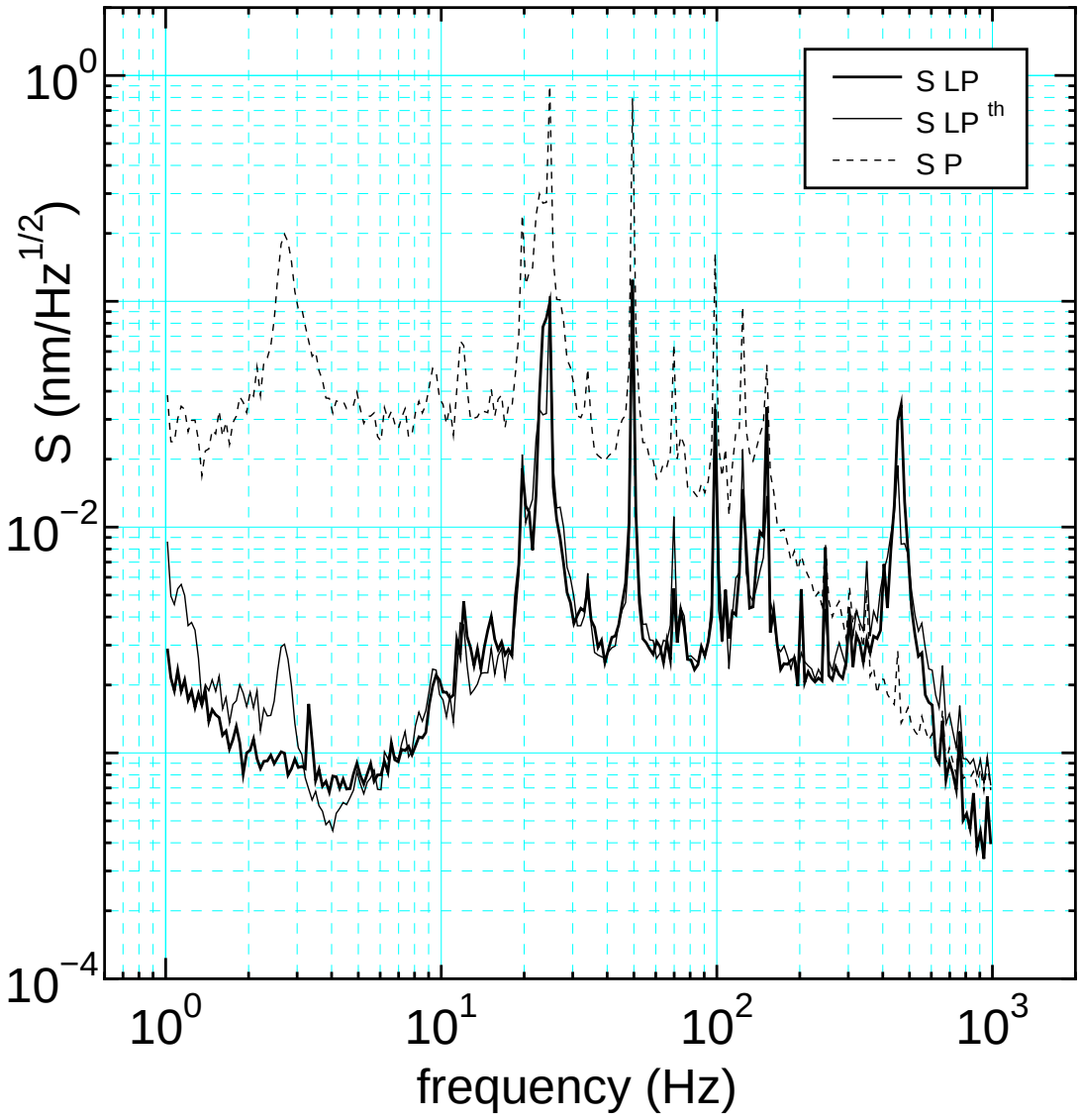

Figure 3.33: power spectrum

power spectrum is about 2 orders, while it is about 0.5 in Fig. 3.25. It is evident that this capability is achieved by Filter2 and Filter3. These positive results prove the effectiveness of improvements done above.

3.3.7 Calibration

We have to convert the unit of output from [V] to [m], which is the unit of optical path length. Maximum and minimum value of the error signal V_{err} is expressed as V_{err}^{max} and V_{err}^{min}. V_{err} is the output of the lock-in amplifier.

V_{err} is expressed using Δphi as follows.

$$V_{err} = \frac{|V_{err}^{max}| + |V_{err}^{min}|}{2} \sin \Delta\phi \tag{3.11}$$

$$= \frac{|V_{err}^{max}| + |V_{err}^{min}|}{2} \sin \frac{\omega \Delta L}{c}. \tag{3.12}$$

We can know the relation between V_{err} and ΔL by differentiating this.

$$\frac{\partial V_{err}}{\partial \Delta L}\Big|_{\Delta L \to 0} = \frac{|V_{err}^{max}| + |V_{err}^{min}|}{2} \cos \frac{\omega \Delta L}{c} \times \frac{\omega}{c}\Big|_{\Delta L \to 0} \tag{3.13}$$

$$= \frac{|V_{err}^{max}| + |V_{err}^{min}|}{2} \frac{\omega}{c} \tag{3.14}$$

$$= \frac{|V_{err}^{max}| + |V_{err}^{min}|}{\lambda} \pi. \tag{3.15}$$

The results and the value of λ is shown in Table. 3.5.

V_{err}^{max} (mV)	V_{err}^{min} (mV)	λ (nm)	$\frac{\partial V_{err}}{\partial \Delta L}$ (mV/nm)
298	-280	1552.4	1.17

Table 3.5: calibration

Therefore, 1.17mV of the error signal corresponds to 1nm of the optical path length. The vertical axis of the power spectrum is calibrated using this value.

3.3.8 Noise of electric circuits

Noise of electric cirsuits was measured to identify the cause of noise in whoke system. First, noise of each circuit element was measured using spectrum analyzer, which is expressed as $S''_{fa}, S''_{f1}, S''_{f2}, S''_{f3}, and S''_{f4}$ in Fig. 3.34.

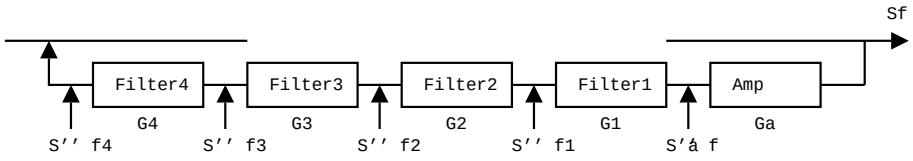

Figure 3.34: noise of each element

S_F, the noise of circuit is calculated using $S''_{fa}, S''_{f1}, S''_{f2}, S''_{f3}$, and S''_{f4} (calculation1).

$$S_F = \left|\frac{G_{LP}}{1+G_{LP}}\right| \left(\frac{S''_{fa}}{G_a} + \frac{S''_{f1}}{G_a G_1} + \frac{S''_{f2}}{G_a G_1 G_2} + \frac{S''_{f3}}{G_a G_1 G_2 G_3} + \frac{S''_{f4}}{G_a G_1 G_2 G_3 G_4} \right) \quad (3.16)$$

S_F can be estimated in another way. Noise of whole circuit was measured, which is expressed as S''_F in Fig. 3.35 (calculation2).

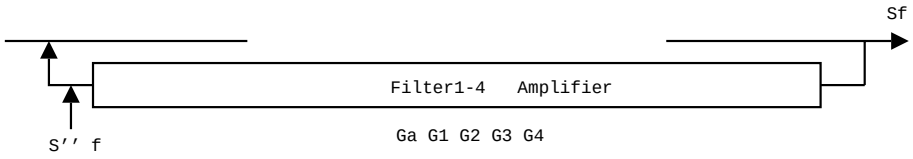

Figure 3.35: noise of all filters and amplifier

S_F, the noise of circuit is calculated using S''_F.

$$S_F = \left|\frac{G_{LP}}{1+G_{LP}}\right| \frac{1}{G_a G_1 G_2 G_3 G_4} S''_F \quad (3.17)$$

These results are shown in Fig. 3.36. The accordance of calculation1 and 2 over 10Hz shows the reliability of this measurement. Although measurement may not have susceeded from 1 to 10Hz, this result implies that the primary cause of noise is that of electric circuits.

3.3.9 Protection against external influence

An optical fiber is thin, is soft and tends to receive influence by external mechanical vibration and temperature fluctuation. We protected the optical system by putting it into a box. A box is a product made from acrylics and is $610 \times 610 \times 310$mm in size. Without this protection, the control was unable. All the experiments above has been done with this box.

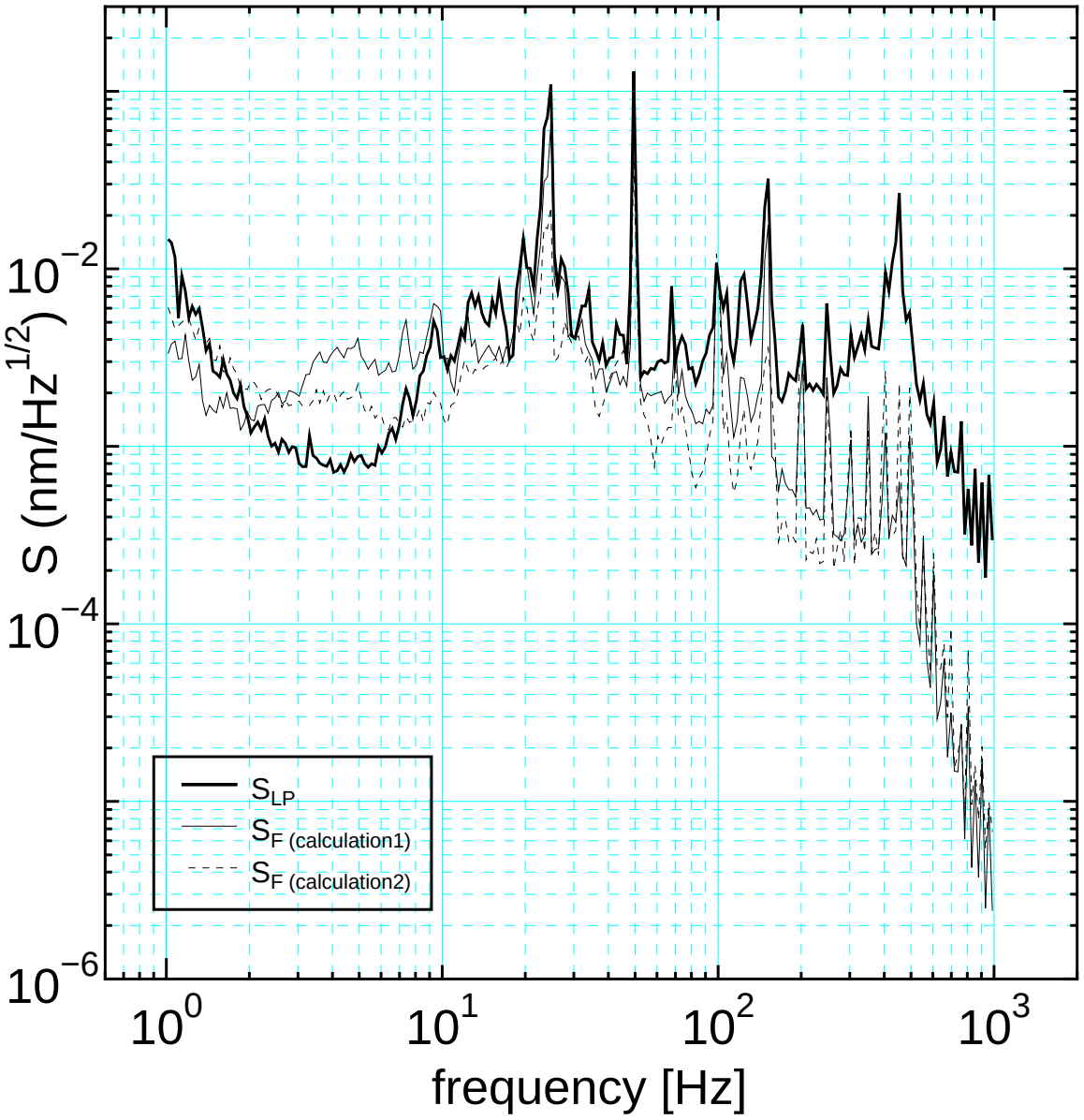

Figure 3.36: cause of noise

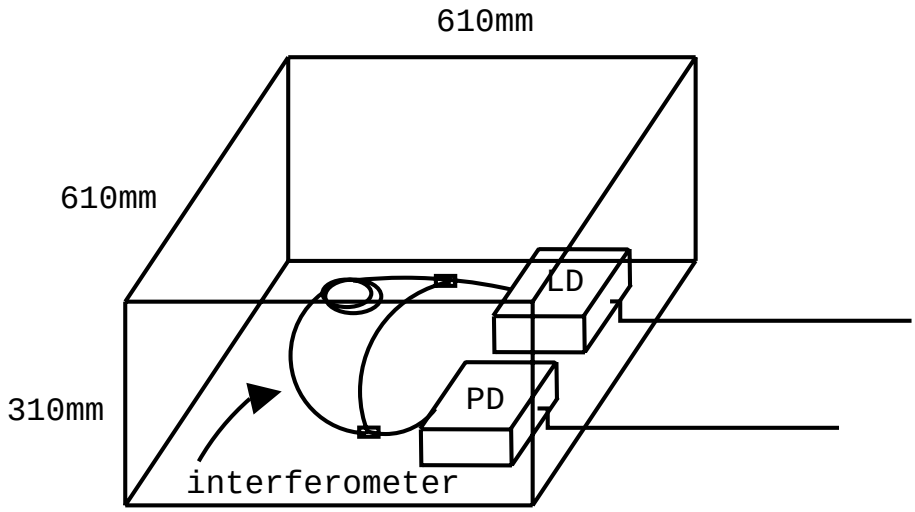

Figure 3.37: the optical system installed in a box

Chapter 4

Conclusions

We have stabilized about 2 orders of laser frequency at the maximum in the 1 to 300Hz zone. Techniques of phase detection using Mach-Zehnder interferometer and phase fixation by 2-loop feedback were used for stabilization.

Below, the figure of a system used for the experiment is shown.

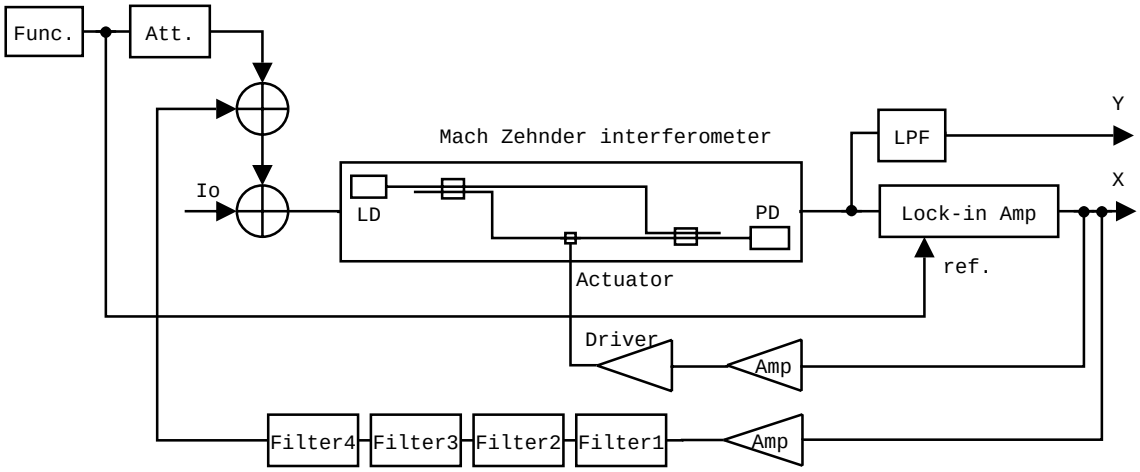

Figure 4.1: 2-loop control with Filter1-4

The stability of laser frequency is expressed with the fall of power spectrum. The result is shown in Fig. 4.2. This figure shows that laser frequency has been stabilized about 2 orders at the maximum in the 1 to 300Hz zone.

Following two are mentioned as a future subject.

- Measurement of absolute stability of laser frequency
  The absolute stability of laser frequency should be measured by using another

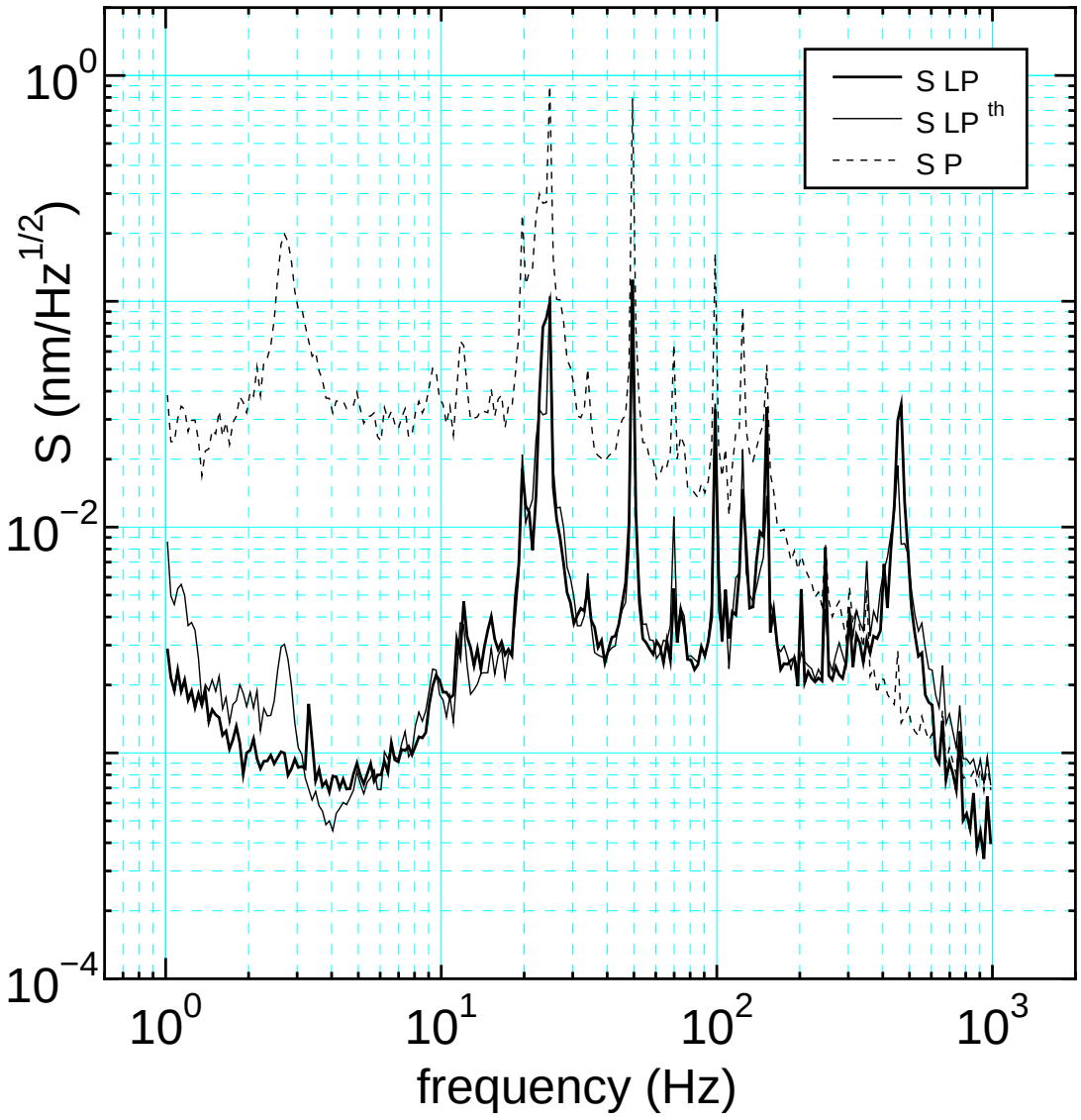

Figure 4.2: power spectrum

interferometer. The system is thought to be as shown in Fig. 4.3. The laser light is split first, and inputted into this interferometer to monitor the absolute stability of laser frequency.

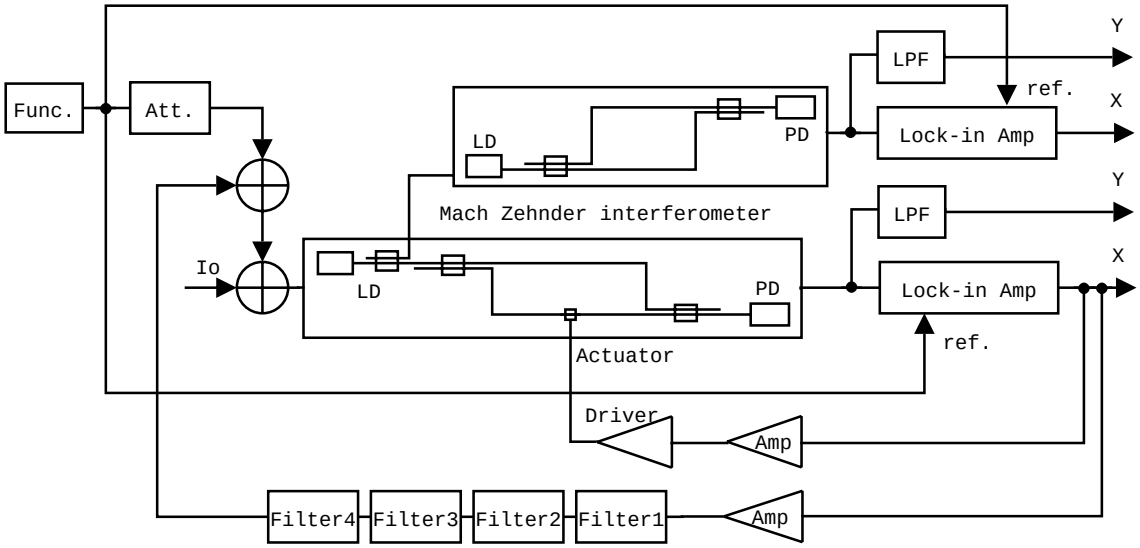

Figure 4.3: the system for monitoring the absolute stability of laser frequency

- Intensity stabilization
  In addition to frequency stabilization, intensity of laser can also be stabilized at the same time. This is probably easier than frequency stabilization. The system is thought to be as shown in Fig. 4.4.

Acknowledgements

First, I would like to thank Prof.Kimio Tsubono who gave us the opportunity to study in a wonderful environment during this term. I am also thankful to Dr.Masaki Ando who led us patiently by much exact advice. I am sure this study could not be completed without help of him. I would also like to thank my college Mr.Hiroshi Yahata. His understanding of the physics and expertise in electric circuit had been a great help to me. It must be also added that some figures in this report were drawn by him.

I owe it entirely to the persons above and many other people who kindly helped me that I was able to complete this study and report. I have no words to thank them for their great kindness.

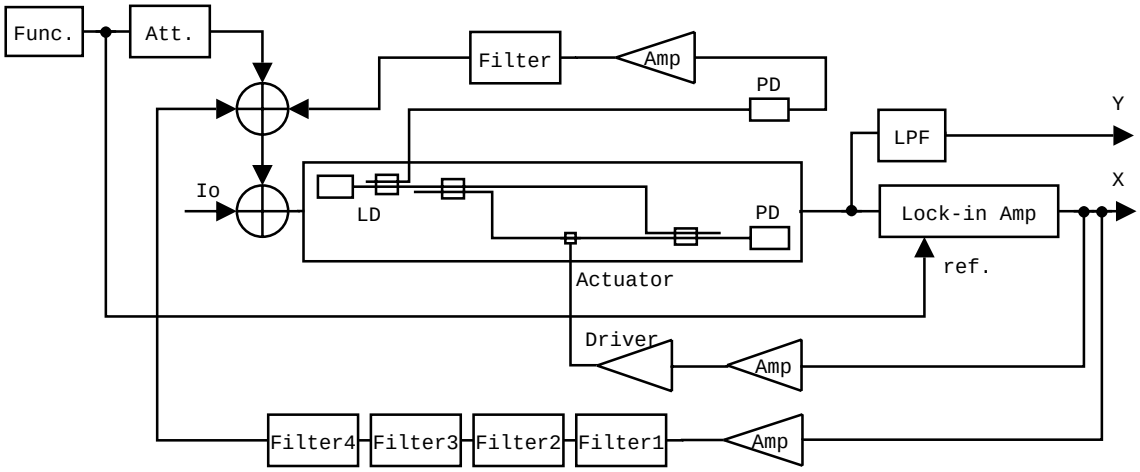

Figure 4.4: the system for intensity stabilization

Appendix

Circuit diagrams

Here, diagrams of circuits of our making are described, which were used in this experiment.

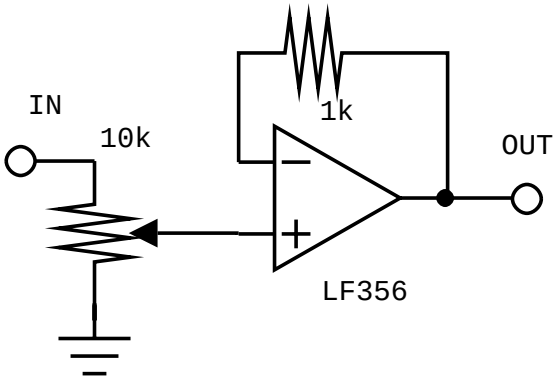

Figure 4.5: Attenuator

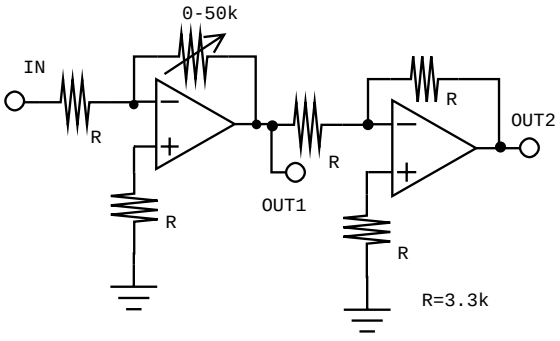

Figure 4.6: Amplifier

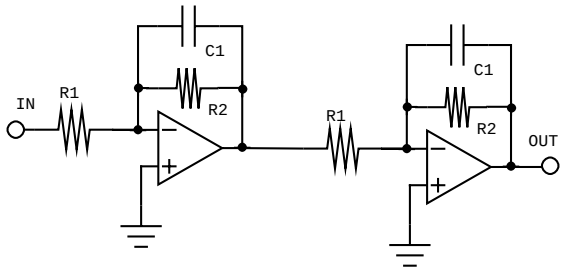

Figure 4.7: Low pass filter

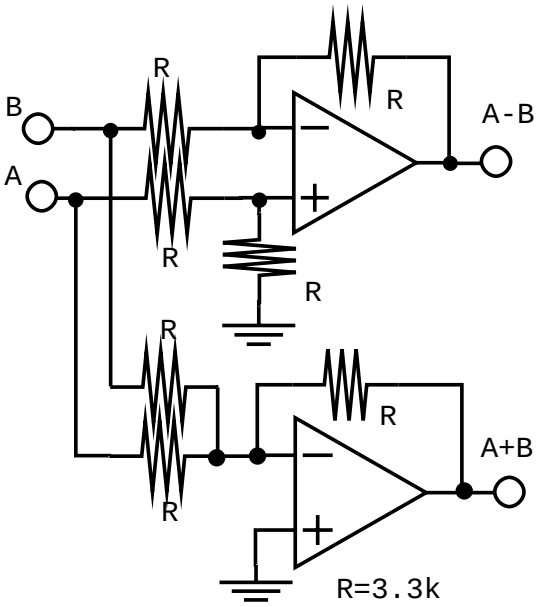

Figure 4.8: Sum amplifier

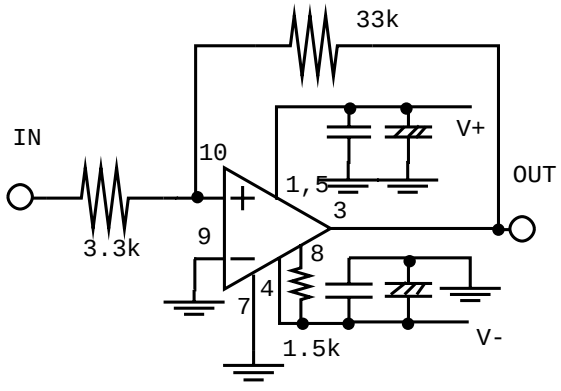

Figure 4.9: Peltier element driver

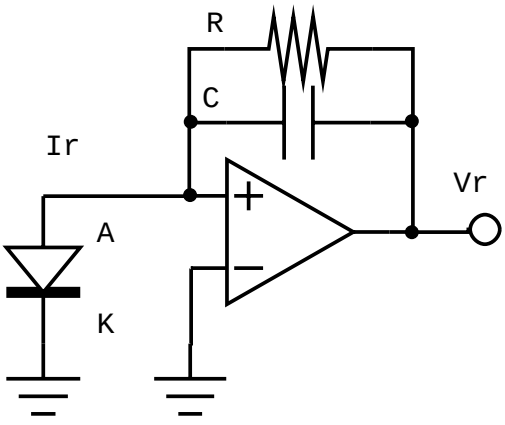

Figure 4.10: Preamplifier

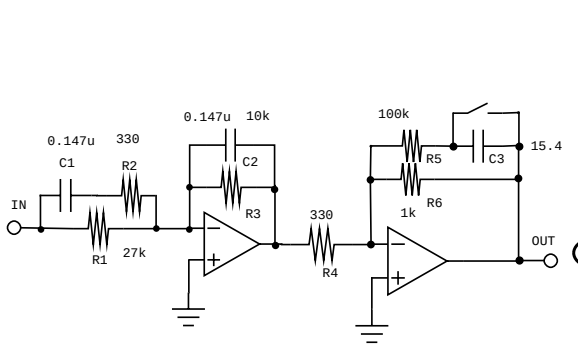

Figure 4.11: Filter1

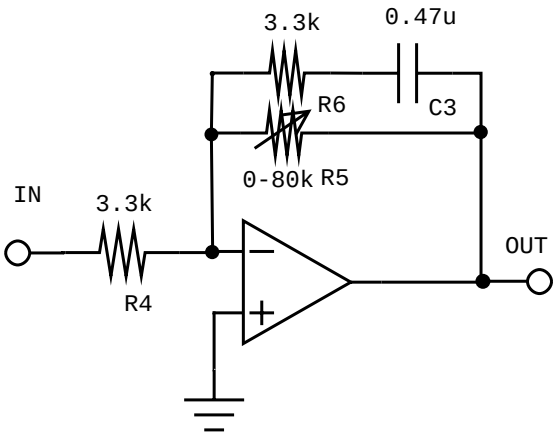

Figure 4.12: Filter2

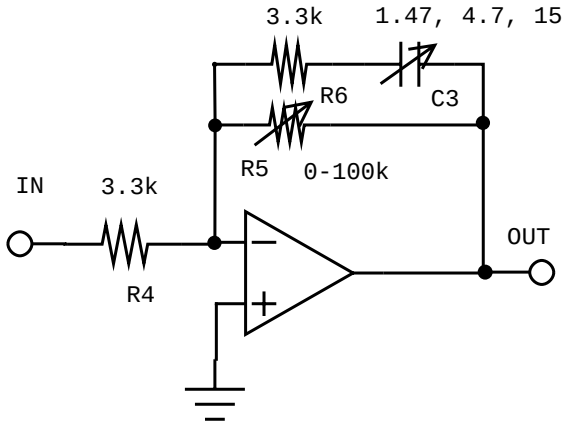

Figure 4.13: Filter3

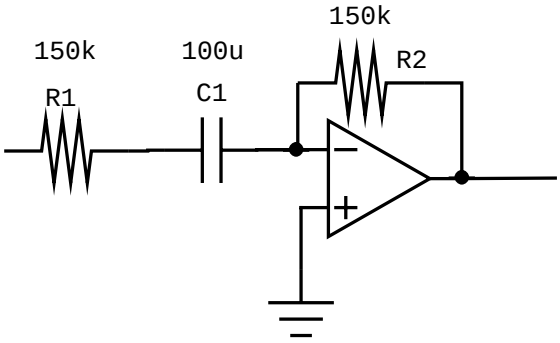

Figure 4.14: Filter4

Bibliography

[1] M.Ando, The control of Fabry-Perot type laser-interferometer gravitational-wave detecter (Master's thesis 1996)

[2] N.Mizukami, Automatic control (Asakura shobou 1971)

[3] Takahiro, Kubota Relativistics (Shoka-bou 2001)

[4] T.Nakamura, Detecting gravitational wave (Kyoto Univ. Press 1998)

[5] I.Ciufolini, and J.A.Wheeler Gravitation and Inertia (Princeton Series in Physics 1995)